Doctoral Dissertation

Tuning the Spin-Orbit Coupling and Transition from the Spin-Singlet to Spin-Triplet State in Non-Centrosymmetric Superconductors $Li_2(Pd_{1-x}Pt_x)_3B$

Shota Harada

GRADUATE SCHOOL
of Natural Science and Technology,

OKAYAMA UNIVERSITY

MARCH 2, 2012

Summary

Spin-orbit interaction has a great importance in condensed materials. Phenomena such as anisotropic magnetoresistance, spin hall effect, multiferroics and so on arises mainly from spin-orbit interaction. The effect of spin-orbit interaction on superconductivity in non-centrosymmetric materials has also attracted much attention. In non-centrosymmetric superconductors, one of the unique characteristics is lack of inversion symmetry. In a superconductor with inversion symmetry, the relation $\psi_{\mathrm{orb}}(\boldsymbol{r}) = \pm\psi_{\mathrm{orb}}(\boldsymbol{r})$ is always true. This derives from the relation $\mathcal{P}^2\psi_{\mathrm{orb}}(\boldsymbol{r}) = \psi_{\mathrm{orb}}(\boldsymbol{r})$, where $\psi_{\mathrm{orb}}(\boldsymbol{r})$ is orbital wave function and $\mathcal{P}$ is the inversion operator. It restricts Cooper pair symmetry to either spin singlet state or spin triplet state due to parity conservation. However, in the case of a non-centrosymmetric superconductor, the relation $\psi_{\mathrm{orb}}(\boldsymbol{r}) \neq \psi_{\mathrm{orb}}(\boldsymbol{r})$ allows a mixing of the spin singlet state and the spin triplet state since the parity conservation is released. The extent of the mixing is considered to be determined by the strength of the spin-orbit coupling.

$Li_2(Pd, Pt)_3B$ shows superconductivity with $T_c \sim 7$ K, 2.7 K, respectively. The crystal structure with distorted octahedral unit has no inversion center in all directions (cubic: $P4_332$, NO. 212). The superconducting gap is isotropic and the Cooper pair is in the spin-singlet state in Li_2Pd_3B, while the gap is anisotropic and Cooper pair is in the spin-triplet state in Li_2Pt_3B. It is considered that the different strength of spin-orbit coupling produces this drastic change of the superconducting properties. However, to obtain detailed insight into the relation between spin-orbit coupling and Cooper pairs symmetry, more investigation is required. In this work, I studied the evolution of Cooper pair's symmetry by tuning the spin-orbit interaction in $Li_2(Pd_{1-x}Pt_x)_3B$. The T_c decreases smoothly with increasing x. The results of the study are as follows:

(1) I have successfully grown samples of $Li_2(Pd_{1-x}Pt_x)_3B$ ($x = 0, 0.2, 0.5, 0.8, 0.84, 0.9, 1$) by the arc melting method. The prepared crystals were checked by XRD to be of high quality.

(2) ^{11}B-NMR:
The temperature dependence of the spin-lattice relaxation rate $^{11}(1/T_1)$ was measured. It was found that $^{11}(1/T_1)$ has coherence peak just below T_c for $x \leq 0.8$ while no coherence peak for $x \geq 0.9$, which indicates that s-wave gap function for $x \leq 0.8$ has been changed to line-node gap function for $x > 0.8$.

(3) ^{195}Pt-NMR:
$^{195}(1/T_1)$ is also measured for $x = 0.84, 0.9, 1$. The results are consistent with $^{11}(1/T_1)$. Temperature dependence of Knight shift ^{195}K was investigated as well. The result shows that the spin-singlet state is dominant for $x \leq 0.8$ whereas the spin triplet state is dominant for $x \geq 0.9$. Furthermore, the mixing-like state was observed for $x = 0.84$.

(4) The NMR investigations show that the superconducting properties suddenly change around $x = 0.8$. To seek the cause for the drastic change, I studied the crystal structure by Rietveld analysis of XRD. I found that the angle of two octahedrons changes dramatically at $x = 0.84$. This result shows that the crystal distortion is the most important to mix the triplet component.

In summary, I found that the crystal structure change as to increase the extent of the distortion is the origin of the spin orbit coupling and the abrupt change of the Cooper pair symmetry at $x = 0.8$.

Contents

Chapter 1

Introduction

In this Chapter, the basic idea on noncentrosymmetryic superconductor is introduced. Superconducting spin symmetry with broken inversion symmetry and the relation with Spin-Orbit Coupling in noncentrosymmetric (NCS) superconductor are remarked. The experimental reports of non-centrosymmetric superconducting properties are introduced as well.

1.1 Symmetry in Superconductors

In this section, spin symmetry of Cooper pair in NCS crystal is discussed.

Spin-orbit interaction has a great importance in condensed matters. Phenomena such as anisotropic magnetoresistance, spin hall effect, multiferroics and so on are caused by spin-orbit interaction, through which the configuration of spins are determined by the orbital symmetry. Naturally, the effect of spin-orbit interaction on superconductivity has been discussed as well. In those systems, one of the unique characteristic is the lack of inversion symmetry. In a superconductor with inversion symmetry, the relation $\psi_{\mathrm{orb}}(\boldsymbol{r}) = \pm\psi_{\mathrm{orb}}(-\boldsymbol{r})$ is always true. This derives from the relation $\mathcal{P}^2\psi_{\mathrm{orb}}(\boldsymbol{r}) = \psi_{\mathrm{orb}}(\boldsymbol{r})$, where $\psi_{\mathrm{orb}}(\boldsymbol{r})$ is the orbital wave function and $\mathcal{P}$ is an inversion operator. This restricts Cooper pair symmetry to either spin singlet state or spin triplet state due to parity conservation. However in the case of a broken inversion superconductor, the relation $\psi_{\mathrm{orb}}(\boldsymbol{r}) \neq \pm\psi_{\mathrm{orb}}(-\boldsymbol{r})$ allows the mixing of the spin singlet state and the spin triplet state [14, 16, 30]. Therefore, the spin symmetry is described by superposition of the two spin states. It is considered that the Cooper pair symmetry is determined by the strength of the spin-orbit coupling. The details will be discussed in the following sections.

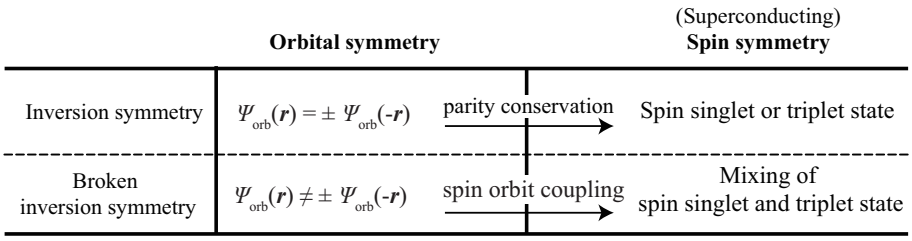

Figure 1.1: Outline drawing of the NCS superconducting spin state.

1.2 Novel Superconducting State

In BCS superconductors, angular momentum $L = 0$, spin angular momentum $S = 0$, wave number $k = 0$. These superconductors are recognized as a conventional superconductor. When $S = 1$ or $k \neq 0$ which are spin triplet state, FFLO state, respectively are known as a novel unconventional superconductor. It is considered that almost all of unconventional superconductors are realized by another electron-electron interaction. These superconductors are expected to show interesting properties because of their internal degree of freedom. However, these superconductor especially spin triplet superconductors are identified in very few materials such as Su_2RuO_4, UPt_3.

Recently, superconducting properties without inversion symmetry have became a hot topics. These superconductors are considered to be another route to realize novel superconductivity.

1.3 Parity Operator

In this section, parity operator are redefined.

Position operator $\hat{r}$ gives the relation

$$\langle r;p|\hat{r}|r;p\rangle = r \tag{1.1}$$
$$\langle -r;p|\hat{r}|-r;p\rangle = -r. \tag{1.2}$$

The $\hat{r}$ takes the position in wave function. When parity operator $\mathcal{P}_r$ which reverses the position is introduced,

$$\langle r;p|\hat{r}|r;p\rangle = \left\langle -r;p\middle|\mathcal{P}_r^\dagger \hat{r}\mathcal{P}_r\middle|-r;p\right\rangle. \tag{1.3}$$

Using the **Equation** (1.2),

$$\mathcal{P}_r^\dagger \hat{r}\mathcal{P}_r = -\hat{r}. \tag{1.4}$$

We can see that $\hat{r}$ is odd under parity transformation for position.

Next, we consider momentum operator $\hat{p}$ as follows,

$$\langle r;p|\hat{p}|r;p\rangle = p \tag{1.5}$$
$$\langle -r;p|\hat{p}|-r;p\rangle = p. \tag{1.6}$$

The $\hat{p}$ gives the momentum in wave function as well. Therefore,

$$\langle r;p|\hat{p}|r;p\rangle = \left\langle -r;p\middle|\mathcal{P}_r^\dagger \hat{p}\mathcal{P}_r\middle|-r;p\right\rangle \tag{1.7}$$

Using the **Equation** (1.6),

$$\mathcal{P}_r^\dagger \hat{p}\mathcal{P}_r = \hat{p}. \tag{1.8}$$

We can see that $\hat{p}$ is even under parity transformation with respect to position. In the same manner, we can define $\mathcal{P}_p$ which is a parity operator with respect to momentum.

As a result, it can be defined $\mathcal{P}$ as

$$\mathcal{P}_r^\dagger \hat{r}\mathcal{P}_r = -\hat{r}, \quad \mathcal{P}_r^\dagger \hat{p}\mathcal{P}_r = \hat{p} \tag{1.9}$$
$$\mathcal{P}_p^\dagger \hat{r}\mathcal{P}_p = \hat{r}, \quad \mathcal{P}_p^\dagger \hat{p}\mathcal{P}_p = -\hat{p} \tag{1.10}$$

Therefore, communicative relations are

$$[\mathcal{P}_r,\hat{r}]_+ = 0, \quad [\mathcal{P}_r,\hat{p}]_- = 0, \quad \left[\mathcal{P}_p,\hat{r}\right]_- = 0, \quad \left[\mathcal{P}_p,\hat{p}\right]_+ = 0. \tag{1.11}$$

In this scheme, we separates Parity operator $\mathcal{P}$ to $\mathcal{P}_r$ and $\mathcal{P}_p$. Namely, we consider that inversion operators with respect to position and momentum are distinguished. Using the relations we can see that angular momentum operator will be asymmetric under the redefined parity operations.

$$\mathcal{P}_r^\dagger \hat{L} \mathcal{P}_r = \mathcal{P}_r^\dagger (\hat{r} \times \hat{p}) \mathcal{P}_r = -\hat{r} \times \hat{p} = -\hat{L} \tag{1.12}$$

$$\mathcal{P}_p^\dagger \hat{L} \mathcal{P}_p = \mathcal{P}_p^\dagger (\hat{r} \times \hat{p}) \mathcal{P}_p = \hat{r} \times -\hat{p} = -\hat{L} \tag{1.13}$$

The communicative relations are

$$\left[\mathcal{P}_r, \hat{L}\right]_+ = 0, \quad \left[\mathcal{P}_p, \hat{L}\right]_+ = 0 \tag{1.14}$$

In the following contents, these operators will be used.

1.4 Parity Conservation and Parity Violation

Generally, it is believed that any physical laws are ruled by parity conservation, which means physical invariance under inversion operation. Any physical equations such as Newton's equation of motion or Maxwell's equations of electromagnetism are considered to be invariant with respect to inversion operation. Parity conservation occupies an important place in any physical properties.

Actually, it have been known that parity conservation do not always consist since the discovery of parity violation in beta decay. In nature, there are a lot of parity violation. For example, almost all of DNA with right-handed helix structure and carbohydrate or amino acid have the unique molecular chirality since these structures cannot accord with the mirrored structures. In solid state materials, it have been known that non-centrosymmetric crystal structure is a typical example of the parity violation.

In quantum mechanics, parity is defined using parity operator $\mathcal{P}$. Since the orbital wave function $\Psi(\boldsymbol{r})$ is subject to a crystal symmetry, $\mathcal{P}\Psi(\boldsymbol{r})$ is transformed to $\Psi(-\boldsymbol{r})$ when $\mathcal{P}$ is added to the orbital wave function. If we act this once again,

$$\mathcal{P}^2\Psi(\boldsymbol{r}) = \Psi(-(-\boldsymbol{r})) = \Psi(\boldsymbol{r}) \tag{1.15}$$

$$\Longrightarrow \mathcal{P}^2 = 1. \tag{1.16}$$

That means $\mathcal{P}$ can take only ± 1. Therefore,

$$\mathcal{P}\Psi(\boldsymbol{r}) = \Psi(-\boldsymbol{r}) = \pm\Psi(\boldsymbol{r}). \tag{1.17}$$

In addition, $\mathcal{P}^2 = 1$ represents that $\mathcal{P}$ is the inverse operator of $\mathcal{P}$. Therefore,

$$\mathcal{P}^\dagger = \mathcal{P}^{-1} = \mathcal{P}. \tag{1.18}$$

If the **Equation** (1.17) consist, it is recognized as centrosymmetric crystal. On the other hand, if the equation does not consist, it is non-centrosymmetric crystal. Non-centrosymmetric system has been a recent hot topic in condensed matter physics.

1.5 Symmetry and Antisymmetry of the Wave Function

The following contents in this section are not targeted only to superconducting state.

Whenever we consider two-electron system such as Cooper pair, one principle must be taken into account. It is general rule named as Pauli exclusion principle, which tells us that electron one quantum state are occupied by only one electron except spin freedom. By this principle, the electron wave function must be antisymmetric considering two electrons are exchanged. In any electronic systems, this principle must be retained since electron is Fermion.

In two-electrons system, the wave function is envisioned as $\Phi(\boldsymbol{r}_1, \boldsymbol{r}_2)$. To see $\Phi(\boldsymbol{r}_1, \boldsymbol{r}_2)$ more clearly, we consider a Hamiltonian bellow,

$$\mathcal{H} = -\frac{\hbar^2}{2m}\Delta_1 + V(|\boldsymbol{r}_1|) - \frac{\hbar^2}{2m}\Delta_2 + V(|\boldsymbol{r}_2|) + \frac{1}{4\pi\epsilon_0}\frac{e^2}{|\boldsymbol{r}_1 - \boldsymbol{r}_2|}. \tag{1.19}$$

The Schrödinger equation gives follows

$$\left[\left\{-\frac{\hbar^2}{2m}\Delta_1 + V(|\boldsymbol{r}_1|)\right\} + \left\{-\frac{\hbar^2}{2m}\Delta_2 + V(|\boldsymbol{r}_2|)\right\} + \frac{1}{4\pi\epsilon_0}\frac{e^2}{|\boldsymbol{r}_1 - \boldsymbol{r}_2|} - E\right]\Phi(\boldsymbol{r}_1, \boldsymbol{r}_2) = 0. \tag{1.20}$$

We expect that $\Phi(\boldsymbol{r}_1, \boldsymbol{r}_2)$ compose from a overlap of each wave function $\phi(\boldsymbol{r}_1)\sigma_1$, $\phi(\boldsymbol{r}_2)\sigma_2$. Therefore, two electron states are described such as $\phi_1(\boldsymbol{r}_1)\alpha_1\phi_2(\boldsymbol{r}_2)\beta_2$, which means that electron labeled as "1" is in $\phi_1(\boldsymbol{r}_1)$ state with spin up, and another electron labeled as "2" is in $\phi_2(\boldsymbol{r}_2)$ state with spin down. Therefore, $\Phi(\boldsymbol{r}_1, \boldsymbol{r}_2)$ can be assumed as,

$$\Phi(\boldsymbol{r}_1, \boldsymbol{r}_2, \sigma_1, \sigma_2) = \frac{1}{\sqrt{2}}\left\{\phi_1(\boldsymbol{r}_1)\sigma_1\phi_2(\boldsymbol{r}_2)\sigma_2 - \phi_2(\boldsymbol{r}_1)\sigma_2\phi_1(\boldsymbol{r}_2)\sigma_1\right\} \tag{1.21}$$

,which preserves the Pauli exclusion principle.

We can consider orbital part and spin part, separately since the Hamiltonian gives no effect in the spin wave function. Therefore, when we exchange the electrons, Pauli principles confine $\Phi(\boldsymbol{r}_1, \boldsymbol{r}_2)$ to

$$\Phi(\boldsymbol{r}_1, \boldsymbol{r}_2)^{\mathrm{s}} = \phi^s(\boldsymbol{r}_1, \boldsymbol{r}_2) \times \chi^a(\sigma_1, \sigma_2) \tag{1.22}$$

$$\Phi(\boldsymbol{r}_1, \boldsymbol{r}_2)^{\mathrm{t}} = \phi^a(\boldsymbol{r}_1, \boldsymbol{r}_2) \times \chi^s(\sigma_1, \sigma_2) \tag{1.23}$$

due to the asymmetricity, where $\phi^s(\boldsymbol{r}_1, \boldsymbol{r}_2)$ and $\chi^s(\sigma_1, \sigma_2)$ are symmetric, $\phi^a(\boldsymbol{r}_1, \boldsymbol{r}_2)$ and $\chi^a(\sigma_1, \sigma_2)$ are antisymmetric orbital and spin function. Practically, $\phi^s(\boldsymbol{r}_1, \boldsymbol{r}_2)$ and $\phi^a(\boldsymbol{r}_1, \boldsymbol{r}_2)$ are written as follows

$$\phi^s(\boldsymbol{r}_1, \boldsymbol{r}_2) = \frac{1}{\sqrt{2}}\left\{\phi_1(\boldsymbol{r}_1)\phi_2(\boldsymbol{r}_2) + \phi_2(\boldsymbol{r}_1)\phi_1(\boldsymbol{r}_2)\right\} \tag{1.24}$$

$$\phi^a(\boldsymbol{r}_1, \boldsymbol{r}_2) = \frac{1}{\sqrt{2}}\left\{\phi_1(\boldsymbol{r}_1)\phi_2(\boldsymbol{r}_2) - \phi_2(\boldsymbol{r}_1)\phi_1(\boldsymbol{r}_2)\right\}. \tag{1.25}$$

And, $\chi^s(\sigma_1, \sigma_2)$ and $\chi^a(\sigma_1, \sigma_2)$ are

$$\chi^s(\sigma_1, \sigma_2) = \begin{cases} \alpha_1\alpha_2, \\ \beta 1 \beta 2, \\ \frac{1}{\sqrt{2}}\left[\alpha_1\beta_2 + \beta_1\alpha_2\right] \end{cases} \tag{1.26}$$

$$\chi^a(\sigma_1, \sigma_2) = \frac{1}{\sqrt{2}}\left[\alpha_1\beta_2 - \beta_1\alpha_2\right]. \tag{1.27}$$

Incidentally, $\chi^s(\sigma_1, \sigma_2)$, $\chi^a(\sigma_1, \sigma_2)$ are known as spin triplet state and spin singlet state, respectively.

The result shows that $\Phi(\boldsymbol{r}_1, \boldsymbol{r}_2)^{\mathrm{s}}$ has only spin singlet state and $\Phi(\boldsymbol{r}_1, \boldsymbol{r}_2)^{\mathrm{t}}$ has only spin triplet state. From only symmetry consideration, the two different spin symmetry ($S = 0, 1$) are determined. Each state exists independently since the transition between the two orbital state is prohibited unless we add magnetic field term into **Equation** (1.20). This is since a spin state remains unchanged through the assumed Hamiltonian.

First, we consider the situation that the wave functions, $\phi(\boldsymbol{r}_1)$, $\phi(\boldsymbol{r}_2)$ have the parity relationship. Therefore we can assume it as follows,

$$\phi(\boldsymbol{r}_2) = \mathcal{P}_r\phi(\boldsymbol{r}_1) = \phi(-\boldsymbol{r}_1) = \pm\phi(\boldsymbol{r}_1). \tag{1.28}$$

We will find that $\Phi(\boldsymbol{r}_1, \boldsymbol{r}_2)^{\mathrm{t}}$ becomes nothing because $\phi^a(\boldsymbol{r}_1, \boldsymbol{r}_2) = 0$ in the **Equation** (1.25). Then we can conclude that spin triplet state does not exist in a centrosymmetric crystal structure. Only spin singlet state realizes.

Next, we consider the situation with parity violation. It is found $\phi^a(\boldsymbol{r}_1, \boldsymbol{r}_2)$ is nonzero in the same manner. Namely, spin triplet state can exists. However the transition between spin singlet and spin triplet state is still prohibited as well since there is no spin operators in **Equation** (1.20). Even under parity violation, it gives no effect to spin states.

When spin-orbit interaction which is discussed in the next section is operated in the Hamiltonian, it is improved as below,

$$\tilde{\mathcal{H}} = \mathcal{H} + \lambda \boldsymbol{L} \bullet \boldsymbol{S}. \tag{1.29}$$

We can not separate the wave function $\Phi(\boldsymbol{r}_1, \boldsymbol{r}_2)$ into orbital part and spin part in that Hamiltonian. However, considering $\lambda = 0$, the wave function must come back to **Equation** (1.20). Therefore the wave function can be improved by first-order perturbation if λ is increased gradually. Immediately, we will see that off-diagonal elements in the Hamiltonian appear because of the occurrence of the transition. We have to diagonalize the matrix elements to obtain the eigen state. The obtained eigen function will be mixing of spin singlet and triplet function. In reality, the interaction is tiny for the first quantum number, $n \leqq 3$. We should take that the hybridization has been prohibited. However if we could increase the interactions, the off-diagonal elements will become large and the hybridization will be unignorable. This is the reason why spin-orbit interaction is important in mixing of spin singlet state and spin triplet state.

However, we need to know one thing about the above explanation. If spin-orbit interaction becomes stronger than electron-electron coulomb interaction, the previous perturbative method gives an incorrect electronic depictions. It means the difficulty to envision electronic state in heavy element by the perturbative theory of the two electron system. In strongly coupled atoms, following route may be the right way to envision it. Firstly, we solve Dirac equation up to second approximation, (first approximation gives Schrödinger equation)

$$(H_{\mathrm{Dirac}} - E)\,\Phi(\boldsymbol{r}, \boldsymbol{\sigma}) = 0 \tag{1.30}$$

where

$$H_{\mathrm{Dirac}} = m_e c^2 + \left[\frac{p^2}{2m_e} - \left(\frac{e^2}{4\pi\epsilon_0}\right)\frac{1}{r}\right] + H_T + H_{SO} + H_D \tag{1.31}$$

$$H_{\mathrm{T}} = -\frac{p^4}{8m_e^3c^2} \tag{1.32}$$

$$H_{\mathrm{SO}} = \left(\frac{e^2}{4\pi\epsilon}\right)\left(\frac{1}{2m_e^2c^2}\right)\boldsymbol{L} \bullet \boldsymbol{S} \tag{1.33}$$

$$H_{\mathrm{D}} = \left(\frac{e^2}{4\pi\epsilon}\right)\left(\frac{\hbar^2\pi}{2m_e^2c^2}\right)\delta(\boldsymbol{r}) \tag{1.34}$$

After getting the eigen function Φ, we expands it to the two electron system and discuss chemical bond secondly. This is because chemical bond are determined by an open shell structure. Therefore, we have to know the structure coupled with spin-orbit interaction at first. Incidentally, H_T, H_{SO} H_D gives correction term for kinetic energy, SO coupling, Darwin term, respectively. In the following sections, only SO coupling will be focused.

1.6 Spin-Orbit Coupling

In this section, the origin and role of spin-orbit interaction, which is a key of non-centrosymmetric superconductor, are introduced to understand the electronic structures [9].

Magnitude of magnetic moment μ which is a consequence of the electronic orbital motion is derived from Bohr magnetron. Spin-orbit Hamiltonian is envisioned as the energy of orientation of this intrinsic magnetic moment in the field produced by the orbital motion of the electron. Therefore,

$$H_{\mathrm{SO}} = -\boldsymbol{\mu}_S \bullet \boldsymbol{B}_{\mathrm{orbital}} \tag{1.35}$$

where $\boldsymbol{\mu}_S$ is the spin magnetic moment given by equation $\boldsymbol{\mu}_S = -(g_e\mu_B/\hbar)\boldsymbol{S}$ and $\boldsymbol{B}$ is the magnetic field produced by orbiting electron. It can be assumed that the B-field is that of the circling proton having speed v. It is required the field at the center of a plane circular loop of radius r. From elementary electromagnetic theory,

$$B_{\mathrm{orbital}} = \frac{\mu_0 i}{2r} \tag{1.36}$$

$$= \frac{i}{\epsilon_0 c^2 2r} \tag{1.37}$$

where the magnetic permeability of free space, μ_0, has been eliminated in favor of electric permittivity of free space ϵ_0 using $\mu_0\epsilon_0 = 1/c^2$. The "current" i is given by

$$i = \frac{ev}{2\pi r}. \tag{1.38}$$

Therefore,

$$B_{\mathrm{orbital}} = \left(\frac{1}{4\pi\epsilon_0}\right)\frac{e}{c^2r^2} \bullet \frac{m_e v r}{m_e r} \tag{1.39}$$

$$= \left(\frac{1}{4\pi\epsilon_0}\right)\frac{e}{m_e c^2 r^3} l. \tag{1.40}$$

Now, it can be calculated as follow

$$H_{\mathrm{SO}} = \left(\frac{1}{4\pi\epsilon_0}\right)\frac{g_e e^2}{2m_e^2 c^2 r^3}\left(\boldsymbol{l} \bullet \boldsymbol{s}\right). \tag{1.41}$$

Inserting the Thomas factor, which is equivalent to dividing **Equation** 1.41 by 2, cancels $g_e = 2$ in the numerator so it is obtained

$$H_{\mathrm{SO}} = \left(\frac{1}{4\pi\epsilon_0}\right)\frac{e^2}{2m_e^2 c^2 r^3}\left(\boldsymbol{l} \bullet \boldsymbol{s}\right) \tag{1.42}$$

$$= \frac{1}{2m_e^2 c^2}\left[\frac{1}{r}\frac{dU(r)}{dr}\right](\boldsymbol{l} \bullet \boldsymbol{s}) \tag{1.43}$$

$$\tag{1.44}$$

where $U(r)$ can be adopted as any central potential energy.

It is customary to represent the coefficient of $\boldsymbol{l} \bullet \boldsymbol{s}$ by $\xi(r)$ so that

$$H_{\mathrm{SO}} = \xi \boldsymbol{l} \bullet \boldsymbol{s} \tag{1.45}$$

where

$$\xi(r) = \frac{1}{2m_e^2c^2}\left[\frac{1}{r}\frac{dU(r)}{dr}\right]. \tag{1.46}$$

The first-order spin-orbit correction to the Bohr energy is

$$\begin{aligned} E_{\mathrm{SO}}^{(1)} &= \langle H_{\mathrm{SO}} \rangle && (1.47)\\ &= \frac{1}{2m_e^2c^2}\left[\left(\frac{e^2}{4\pi\epsilon_0}\right)\left\langle\frac{1}{r^3}\right\rangle\right]\langle \boldsymbol{l} \bullet \boldsymbol{s}\rangle && (1.48)\\ &= \frac{1}{2m_e^2c^2}\left(\frac{e^2}{4\pi\epsilon_0}\right)\frac{1}{a_0^3}\left\{\frac{[j(j+1)-l(l+1)-3/4]}{2n^3l(l+1/2)(l+1)}\hbar^2\right\} && (1.49)\\ &= -\frac{1}{2n}\alpha^2 E_n^{(0)}\frac{[j(j+1)-l(l+1)-3/4]}{[l(l+1/2)(l+1)]} && (1.50) \end{aligned}$$

where

$$\begin{aligned} \alpha &= \frac{e^2}{(4\pi\epsilon_0)\hbar c} \simeq \frac{1}{137} && (1.51)\\ a_0 &= (4\pi\epsilon_0)\frac{\hbar^2}{m_e e^2} && (1.52)\\ E_n^{(0)} &= -\frac{1}{2}\alpha^2\frac{m_e c^2}{n^2} && (1.53)\\ \left\langle\frac{1}{r^3}\right\rangle &= \frac{1}{a_0^3} && (1.54)\\ \langle \boldsymbol{l} \bullet \boldsymbol{s}\rangle &= \frac{1}{2}\left\langle n, j, m_j, l, s\right|\left(J^2 - L^2 - S^2\right)\left|n, j, m_j, l, s\right\rangle && (1.55)\\ &= \frac{1}{2}\left[j(j+1)-l(l+1)-3/4\right]\hbar^2 && (1.56) \end{aligned}$$

were used.

For hydrogen j can take on only tow values, $l \pm 1/2$, so the spin-orbit correction is expressed in terms of l for each of these values of j. We have

$$\begin{aligned} \left(E_{\mathrm{SO}}^{(1)}\right)_{n,j=l+\frac{1}{2}} &= -\frac{1}{2n}\alpha^2 E_n^{(0)}\frac{1}{\left[(l+\frac{1}{2})(l+1)\right]} && (1.57)\\ \left(E_{\mathrm{SO}}^{(1)}\right)_{n,j=l-\frac{1}{2}} &= \frac{1}{2n}\alpha^2 E_n^{(0)}\frac{1}{\left[l(l+\frac{1}{2})\right]}. && (1.58) \end{aligned}$$

Inserting the spin-orbit interaction in general hydrogen energy level, the energy spectrum is shifted as given in **Fig**. 1.2. It is noticed that not only p levels but also s levels are shifted. The shifts of p levels are due to the spin-orbit interaction. However that of s levels are not due to the spin orbit interaction since the spin-orbit coupling Hamiltonian is proportional to $\boldsymbol{l} \bullet \boldsymbol{s}$ so it vanishes for s states, which is in $l = 0$ state. The shift of s levels are due to Darwin term $\mathcal{H}_D$ which is valid only for s-state because of the δ function. Incidentally, a coupled ket $|n00\rangle$ are eigenkets of H_D and

$$E_{\mathrm{D}}^{(1)} = \left(\frac{e^2}{4\pi\epsilon_0}\right)\frac{\hbar^2\pi}{2m_e^2c^2}\langle n00|\,\delta(r)\,|n00\rangle\,. \tag{1.59}$$

We do not have to be nervous about the interaction since H_{D} is valid only s orbital, it cannot be a key interaction of novel phenomena.

In the hydrogen model, the actual spin-orbit interaction is ignorable. However, it will become considerable interaction with increasing atomic number Z. Considering the Coulomb potential for the one-electron atom

$$U(r) = -\frac{Ze^2}{4\pi\epsilon_0} \bullet \frac{1}{r} \tag{1.60}$$

where Z is atomic number. Therefore, modifications are required for $\langle H_{\mathrm{SO}} \rangle$ as follows,

$$E_{\mathrm{SO}}^{(1)} = \langle H_{\mathrm{SO}} \rangle = \frac{Z}{2m_e^2c^2}\left[\left(\frac{e^2}{4\pi\epsilon_0}\right)\left\langle\frac{1}{r^3}\right\rangle\right]\langle \boldsymbol{l} \bullet \boldsymbol{s} \rangle . \tag{1.61}$$

Since $\left\langle 1/r^3 \right\rangle$ is in proportion to Z^3 using Table 1.1, it is expressed as

$$E_{\mathrm{SO}}^{(1)} = \frac{Z^4}{2m_e^2c^2}\left(\frac{e^2}{4\pi\epsilon_0}\right)\frac{1}{a_0^3}\left\{\frac{[j(j+1) - l(l+1) - 3/4]}{2n^3 l(l+1/2)(l+1)}\hbar^2\right\}. \tag{1.62}$$

Generally spin-orbit interaction is in proportion to Z^4, which means that it is of considerable importance in heavy elements.

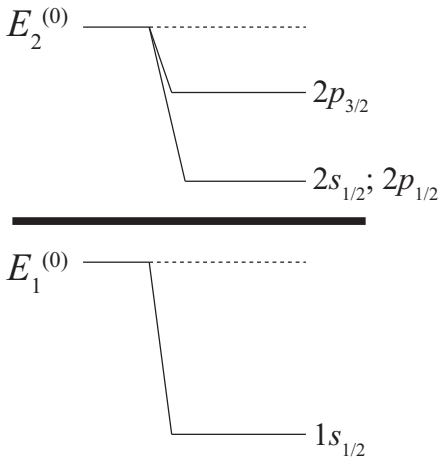

Figure 1.2: Energy splits by spin-orbit interaction in hydrogen atom.

1.7 Multielectron System

1.7.1 spin-orbit coupling in multielectron system

The spin-orbit interaction in multielectron system can be envisioned as follows,

$$\mathcal{H}_{\mathrm{SO}} = \sum_j \xi_j(\boldsymbol{l}_j \bullet \boldsymbol{s}_j). \tag{1.63}$$

$$\left\langle r^2 \right\rangle = \left(\frac{a_0}{Z}\right)^2 \left\{\frac{n^2}{2}\left[5n^2 + 1 - 3l(l+1)\right]\right\}$$
$$\langle r \rangle = \left(\frac{a_0}{Z}\right)\left\{\frac{1}{2}\left[3n^2 - l(l+1)\right]\right\}$$
$$\left\langle r^{-1} \right\rangle = \frac{1}{(a_0/Z)}\left(\frac{1}{n^2}\right)$$
$$\left\langle r^{-2} \right\rangle = \frac{1}{(a_0/Z)^2}\left\{\frac{1}{n^3\,(l+1/2)}\right\}$$
$$\left\langle r^{-3} \right\rangle = \frac{1}{(a_0/Z)^3}\left\{\frac{1}{n^3 l\,(l+1/2)\,(l+1))}\right\}$$
$$\left\langle r^{-4} \right\rangle = \frac{1}{(a_0/Z)^4}\left(\frac{1}{2}\right)\left\{\frac{3n^2 - l(l+1)}{n^5 l\,(l-1/2)\,(l+1/2)\,(l+1)\,(l+3/2)}\right\}$$

Table 1.1: Expectation value of r^s for one-electron atoms

It is already demonstrated that the **Equation** (1.63) can be deformed using total angular momenta $\boldsymbol{L}$, $\boldsymbol{S}$. Therefore,

$$\begin{aligned} H_{\mathrm{SO}} &= \sum_j \xi_j(\boldsymbol{L}_j \bullet \boldsymbol{s}_j). \\ &= \lambda \boldsymbol{L} \bullet \boldsymbol{S} && (1.64) \\ &= \frac{\lambda}{2}\left(\boldsymbol{J^2} - \boldsymbol{L}^2 - \boldsymbol{S}^2\right) && (1.65) \\ &= \frac{\lambda}{2}\left[J(J+1) - L(L+1) - S(S+1)\right] && (1.66) \end{aligned}$$

where λ is,

$$\lambda = \frac{\xi}{n} = \frac{\xi}{2S} \qquad 1 \leqq n \leqq 2l+1 \qquad (1.67)$$
$$\lambda = -\frac{\xi}{2(2l+1) - n} = -\frac{\xi}{2S} \qquad 2l+1 < n < 2\,(2l+1)\,. \qquad (1.68)$$

It is noted that λ can be a positive or negative value. It is helpful to think of the holes as having magnetic moments in the opposite direction to that of the electrons. Therefore, when electron is dominant, $\lambda = \xi/2S \geq 0$ and when hole is dominant, $\lambda = -\xi/2S \leq 0$. For a level that is half-filled, the spin-orbit coupling will vanish.

In multielectron system, we have to consider the magnitude relation between H_{rep} and H_{SO} where H_{rep} originates from electron-electron coulomb interaction (interelectron coulomb interaction).

1.7.2 *L*-*S* coupling

In multielectron system, it is convenience to use term symbol. A quantum state are designated by the vector sum of all the orbital and spin angular momenta, L, S and J, the vector sum of L and S. Therefore, the term symbol designation is

$$^{2S+1}L_J \qquad (1.69)$$

where J can take $J = |L+S|, |L+S-1|, |L+S-2|, ...|L-S|$.

If the Hamiltonian does not include spin-orbit coupling, the state has $(2S + 1)(2L + 1)$-fold degeneracy. However, Hunt rule (Rule 1 and Rule 2), which originates from interelectron coulomb interaction, should be take into account.

Rule 1:
For states composed of equivalent electrons, the state of highest S lies lowest.

Rule 2:
For a given S with the same configuration of equivalent electrons, the state with the highest L lies lowest.

If we applies spin-orbit coupling perturbatively, the spin-orbit interaction will break the degeneracy and select the ground state among them. The ground state is determined by following rule (Rule 3).

Rule 3:
For a given multiplicity and value of L, the state having the lowest J lies lowest for subshells that are less than half-full. If the subsell is more than half-full the state having the highest value of J lies lowest.

When the spin-orbit coupling is weaker than electron-electron coulomb interaction, the procedure can be applied because Hunt rule has priority over Rule 3. This scheme is widely known as Russell-Saunders coupling (L-S coupling).

For instance, the electronic configurations of d orbital are presented in Table 1.2.

$m_L =$	-2	-1	0	1	2	L	S	$L \pm S$	ground state
$(nd)^0$						0	0	0	$^1S_0$
$(nd)^1$					↓	2	1/2	3/2	$^2D_{3/2}$
$(nd)^2$				↓	↓	3	1	2	$^3F_2$
$(nd)^3$			↓	↓	↓	3	3/2	3/2	$^4F_{3/2}$
$(nd)^4$		↓	↓	↓	↓	2	2	0	$^5D_0$
$(nd)^5$	↓	↓	↓	↓	↓	0	5/2	5/2	$^6S_{5/2}$
$(nd)^6$	↑↓	↓	↓	↓	↓	2	4	4	$^5D_4$
$(nd)^7$	↑↓	↑↓	↓	↓	↓	3	3/2	9/2	$^4F_{9/2}$
$(nd)^8$	↑↓	↑↓	↑↓	↓	↓	3	1	4	$^3F_4$
$(nd)^9$	↑↓	↑↓	↑↓	↑↓	↓	2	1/2	5/2	$^2D_{5/2}$
$(nd)^{10}$	↑↓	↑↓	↑↓	↑↓	↑↓	0	0	0	$^1S_0$

Table 1.2: Electronic configurations of d orbital ruled by L-S coupling

1.7.3 j-j coupling

When spin-orbit coupling is stronger than electron-electron coulomb interaction, Rule 3 determines a major trend of the electronic system. Namley, Fund rule can be applied secondly. The scheme is named as j-j coupling. In this scheme, the minimum (or

maximum) J gives the lowest energy state. Therefore, in j-j-coupling, the eigen wave function is designated by J andM_J,

$$\left|J, M_J\right\rangle = \sum_{m_1=-j_1}^{j_1} \sum_{m_2=-j_2}^{j_2} C_{j_1 j_2, J, M_J} \psi_{j_1, m_1} \psi_{j_2, m_2}. \tag{1.70}$$

To see the difference between L-S coupling and j-j coupling, we will take $(np)^2$ state. The term symbol has ${}^1S_0$, ${}^3P_{0,1,2}$, ${}^1D_2$. In L-S coupling scheme, the energy level diagram is ${}^3P_0 < {}^3P_1 < {}^3P_2 < {}^1D_2 < {}^1S_0$ while in j-j coupling scheme, ${}^3P_0 < {}^1S_0 < {}^3P_1 < {}^3P_2 < {}^1D_2$ (see Fig 1.3, [23]). The results are completely different. Therefore, we should consider which scheme is better to describe an electronic state correctly.

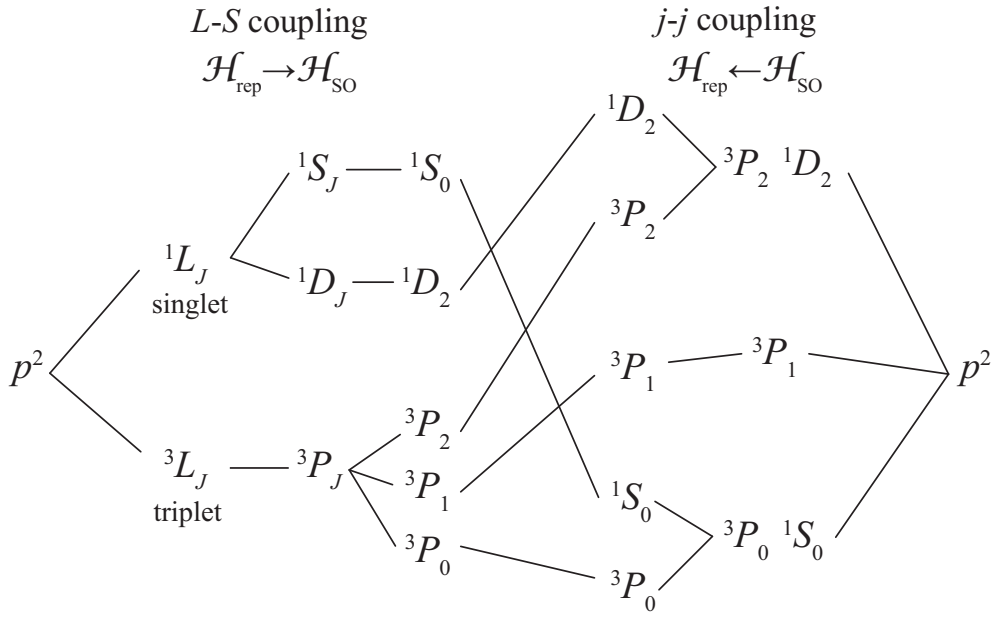

Figure 1.3: Energy correlation diagram of L-S coupling and j-j coupling in p^2 configuration

1.8 Asymmetric Spin-Orbit Coupling (ASOC)

In the above discussion, it was considered that the effect of spin-orbit interaction into multielectron for single atom. Namely, it was a story about electronic core structure. Free electron, which determines actual physical character, runs on the structure which is arranged on the basis of a crystal symmetry. In the following, the spin-orbit interaction on one free electron in centrosymmetric or non-centrosymmetric crystal structure will be considered. We will see that the spin-orbit interaction vanishes in centrosymmetric crystal structure while it survives in non-centrosymmetric structure.

First, we can defines $|\Phi\rangle$ as

$$|\Phi\rangle = \left|J, M_J\right\rangle + \sum_{k=0}^{\infty} \left(c_k |k\rangle + c_{-k} |-k\rangle\right) \sum_{\sigma=\pm} \Gamma_\sigma |\sigma\rangle \tag{1.71}$$

$$= \left|J, M_J\right\rangle + \left|\psi, \gamma\right\rangle \tag{1.72}$$

where

$$\left|\psi\right\rangle = \sum_{k=-\infty}^{\infty} c_k \left|k\right\rangle = \sum_{k=0}^{\infty} \left(c_k \left|k\right\rangle + c_{-k} \left|-k\right\rangle\right) \tag{1.73}$$

$$\left|\gamma\right\rangle = \Gamma_\sigma \left|\sigma\right\rangle . \tag{1.74}$$

The expected value of $\lambda \boldsymbol{L} \bullet \boldsymbol{S}$ is written as follows,

$$\begin{aligned}\langle \lambda \boldsymbol{L} \bullet \boldsymbol{S} \rangle = \frac{\lambda}{2} \{J(J+1) - L(L+1) - S(S+1)\} \\ + \langle \psi | \lambda \boldsymbol{L} | \psi \rangle \bullet \langle \gamma | \boldsymbol{S} | \gamma \rangle\end{aligned} \tag{1.75}$$

where we can define that the first and second terms give core electron energy and free electron energy, respectively. Incidentally, it is expected that the core electron energy will change chemical potential, and within the given J the free electron will move. We will focus on the orbital integral in the free electron term, which is

$$\langle \psi | \lambda \boldsymbol{L} | \psi \rangle = \sum_{k=0}^{\infty} \sum_{k'=0}^{\infty} \left(c_{k'}^* \langle k' | + c_{-k'}^* \langle -k' |\right) \lambda \boldsymbol{L} \left(c_k \left|k\right\rangle + c_{-k} \left|-k\right\rangle\right) \tag{1.76}$$

$$\begin{aligned}= \sum_{k=0}^{\infty} \sum_{k'=0}^{\infty} \Big\{ & c_{k'}^* c_k \langle k' | \lambda \boldsymbol{L} | k \rangle + c_{-k'}^* c_{-k} \langle -k' | \boldsymbol{L} | -k \rangle \\ & + c_{k'}^* c_{-k} \langle k' | \lambda \boldsymbol{L} | -k \rangle + c_{-k'}^* c_k \langle -k' | \lambda \boldsymbol{L} | k \rangle \Big\}.\end{aligned} \tag{1.77}$$

Considering inversion operation $\mathcal{P}_r$ in the system,

$$\mathcal{P}_r \left|\psi\right\rangle = \sum_{k=0}^{\infty} c_k \mathcal{P}_r \left|k\right\rangle + c_{-k} \mathcal{P}_r \left|-k\right\rangle \tag{1.78}$$

$$= \sum_{k=0}^{\infty} c_k \left|-k\right\rangle + c_{-k} \left|k\right\rangle . \tag{1.79}$$

where

$$\mathcal{P}_r \left|k\right\rangle = \mathcal{P}_k \left|k\right\rangle = \left|-k\right\rangle , \quad \mathcal{P}_r \left|-k\right\rangle = \mathcal{P}_k \left|-k\right\rangle = \left|k\right\rangle \tag{1.80}$$

are used. This is since crystal wave function must be periodic and thus

$$\left|k\right\rangle \equiv e^{ikx} \tag{1.81}$$

$$\mathcal{P}_r \left|k\right\rangle = e^{-ikx} = \mathcal{P}_k \left|k\right\rangle . \tag{1.82}$$

In a centrosymmetric structure,

$$\left|\psi\right\rangle = \mathcal{P}_r \left|\psi\right\rangle \tag{1.83}$$

,which gives that

$$c_{-k} = \pm c_k. \tag{1.84}$$

Therefore,

$$\begin{aligned}\langle \Phi | \lambda \boldsymbol{L} | \Phi \rangle = \sum_{k=0}^{\infty} \sum_{k'=0}^{\infty} c_{k'}^* c_k \Big[& \{\langle k' | \lambda \boldsymbol{L} | k \rangle + \langle -k' | \lambda \boldsymbol{L} | -k \rangle\} \\ & \pm \{\langle k' | \lambda \boldsymbol{L} | -k \rangle + \langle -k' | \lambda \boldsymbol{L} | k \rangle\} \Big]\end{aligned} \tag{1.85}$$

$$= \sum_{k=0}^{\infty} \sum_{k'=0}^{\infty} c_{k'}^* c_k \left[\left\langle k' \right| \lambda \left\{ \boldsymbol{L} + \mathcal{P}^\dagger \boldsymbol{L} \mathcal{P} \pm (\boldsymbol{L}\mathcal{P} + \mathcal{P}^\dagger \boldsymbol{L}) \right\} \left| k \right\rangle \right]. \tag{1.86}$$

Using the communicative relation in the **Equation** (1.14),

$$= \sum_{k=0}^{\infty}\sum_{k'=0}^{\infty} c_{k'}^{*}c_k\left[\left\langle k'\right|\lambda\left\{\boldsymbol{L}-\boldsymbol{L}\mathcal{P}^{\dagger}\mathcal{P}\pm(\boldsymbol{L}\mathcal{P}-\boldsymbol{L}\mathcal{P}^{\dagger})\right\}\left|k\right\rangle\right] \tag{1.87}$$

$$= \sum_{k=0}^{\infty}\sum_{k'=0}^{\infty} c_{k'}^{*}c_k\left[\langle k'|\lambda\{\boldsymbol{L}-\boldsymbol{L}\pm(\boldsymbol{L}\mathcal{P}-\boldsymbol{L}\mathcal{P})\}|k\rangle\right] \tag{1.88}$$

$$= 0 \tag{1.89}$$

We can find that when there is the inversion operator in a crystal space group, the free electron feels no spin-orbit interaction. For the discussion of the spin-orbit interaction, non-centrosymmetric structure is requisite.

Incidentally if we defines $\alpha\boldsymbol{g}_{k',k}$ as

$$\alpha\boldsymbol{g}_{k',k} \equiv \langle k'|\lambda\boldsymbol{L}|k\rangle\,, \tag{1.90}$$

the **Equation** (1.77) will be

$$\langle\psi|\lambda\boldsymbol{L}|\psi\rangle = \sum_{k=-\infty}^{\infty}\sum_{k'=-\infty}^{\infty}\alpha c_{k'}^{*}c_k\boldsymbol{g}_{k',k} = \sum_{k=-\infty}^{\infty}\alpha c_k^{*}c_k\boldsymbol{g}_k. \tag{1.91}$$

where

$$\boldsymbol{g}_k = \sum_{k'=-\infty}^{\infty}\boldsymbol{g}_{k',k} = \boldsymbol{g}_{k,k} \tag{1.92}$$

It seems that when $\boldsymbol{g}_k^{\mathrm{ASO}} = -\boldsymbol{g}_{-k}^{\mathrm{ASO}}$, the spin-orbit interaction is named as asymmetric spin-orbit coupling (ASOC). It means that $\boldsymbol{g}_k^{\mathrm{ASO}}$ is odd with respect to $P_k(=P_p)$,

$$\alpha\boldsymbol{g}_k^{\mathrm{ASO}} = \langle k|\lambda\boldsymbol{L}|k\rangle = \left\langle -k\right|P_k^{\dagger}\lambda\boldsymbol{L}P_k\left|-k\right\rangle \tag{1.93}$$

$$\Longrightarrow = -\langle -k|\lambda\boldsymbol{L}|-k\rangle = -\alpha\boldsymbol{g}_{-k}^{\mathrm{ASO}}. \tag{1.94}$$

The ASOC is in the center of the discussion about the mixing of the spin-singlet and spin-triplet states.

1.9 Band structure under ASOC

Within usual no spin-orbit coupling, either up and down spins gives the same energy band state since it is determined by only the orbital component of wave function. Therefore,

$$E(k)\langle\alpha|\alpha\rangle = E(-k)\langle\beta|\beta\rangle = E(k)\langle\beta|\beta\rangle = E(-k)\langle\alpha|\alpha\rangle\,. \tag{1.95}$$

The **Equation** (1.95) is described in **Fig**. 1.4 (a). As discussed previously, a finite spin-orbit interaction will disappears by parity operation. So, if there is inversion symmetry in a crystal, the band structure will be **Fig**. 1.4 (a) as well, regardless of finite spin-orbit interaction. Therefore we assume non-centrosymmetric crystal system in the followings.

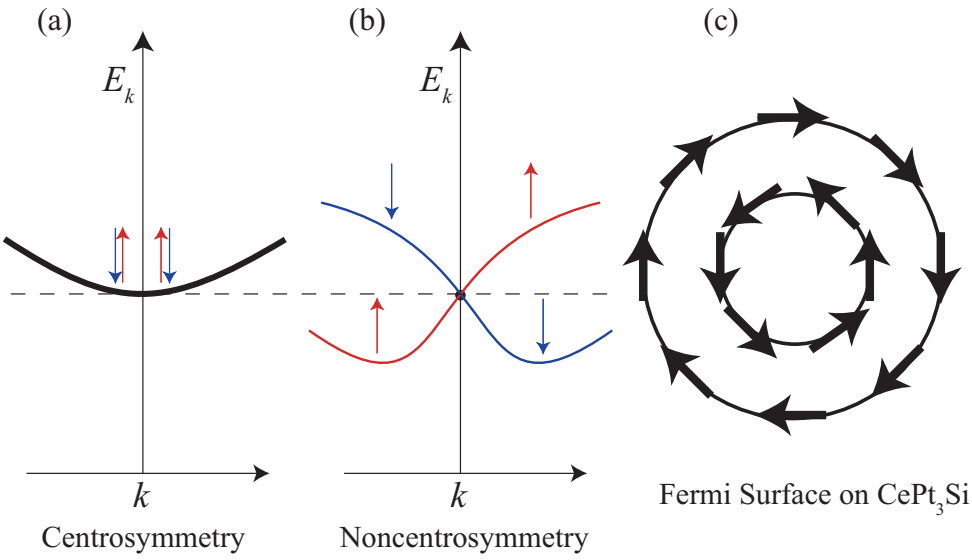

Figure 1.4: Effect of spin-orbit coupling into band structures.(a) Spin-orbit couping is absent or both spin-orbit coupling and inversion center are present. (b) Spin-orbit coupling is present but inversion center is absent. It is expected that $CePt_3Si$ with lack of inversion parallel to c axis has this band structure. (c) An example of two-dimensional Fermi surfaces splitted by Rashba spin-orbit interaction depicted on the k_x-k_y plane [15].

Considering spin-orbit interaction, the band degeneracy breaks except $k = 0$,

$$E(k)\langle\alpha|\alpha\rangle \neq E(k)\langle\beta|\beta\rangle\,, \quad E(-k)\langle\alpha|\alpha\rangle \neq E(-k)\langle\beta|\beta\rangle \tag{1.96}$$

However considering a simple situation that ASOC has a lack of inversion parallel to z axis, we can imagine that down spin with $\boldsymbol{k}$ and up spin with $-\boldsymbol{k}$ (or up spin with $\boldsymbol{k}$ and down spin with $-\boldsymbol{k}$) have same energy since

$$\tilde{E}_k = \sum_{k',\sigma'}\langle k',\sigma'|H_{SO}|k,\beta\rangle = \alpha g^z_k\langle\beta|S^z|\beta\rangle = -\alpha' g^z_k \tag{1.97}$$

$$\tilde{E}_{-k} = \sum_{k',\sigma'}\langle k',\sigma|H_{SO}|-k,\alpha\rangle = \alpha g^z_{-k}\langle\alpha|S^z|\alpha\rangle = \alpha' g^z_{-k} = -\alpha' g^z_k \tag{1.98}$$

Therefore,

$$E(k)\langle\alpha|\alpha\rangle = E(-k)\langle\beta|\beta\rangle\,, \quad E(-k)\langle\alpha|\alpha\rangle = E(k)\langle\beta|\beta\rangle\,. \tag{1.99}$$

The **Equation** (1.99) is also described in **Fig**. 1.4 (b). There is a couple of energy bands at Fermi surface which is characterized by a spin orientation (**Fig**. 1.4 (c), [15]). The situation is applicable to NCS superconductor $CePt_3Si$ which lacks inversion parallel to *c* axis.

1.10 Experimental Report on NCS Superconducting Properties

In this section, some reports about $Li_2(Pd,Pt)_3B$ will be demonstrated, which is categorized into $5d$ electron system. Advantages to study $Li_2(Pd,Pt)_3B$ are remarked.

1.10.1 Categorization of NCS materials

In order to understand the NCS superconductors, we need accurate investigations because of the complex behaviors. In the followings, what are suitable material to progress the study is remarked.

Some materials can be categorized into two groups. One is heavy fermion superconductor with f electron system such as $CePt_3Si$ [7], UIr [1] $Ce(Rh,Ir)_3Si$ [21, 34]. Since f electrons are close to atomic core, they tend to be a localized electron. It is named as heavy fermion electronic system because the electrons are bound by core strongly, and therefore, we must pay heavy costs to bring them outside. Also, they do not contribute to chemical bonding. Therefore, the f-electrons interact through exchange interaction between f-s,p,d. For this reason, f electron system is insensitive to their crystal symmetry. These materials have a characteristic feature that the superconductivity appears after a magnetic order. Electronic system including f-electrons is very complicated because coulomb interactions and spin-orbit interaction must be taken into account all together.

Another group is d electron system such as $Mg_{10}Ir_{19}B_{16}$ [22, 37], Ir_2Ga_9 [31], Re_3W [39], $BaPtSi_3$ [8], $Ca(Ir, Pt)_3$ [12] and $Li_2(Pd, Pt)_3B$ [38] with itinerant electrons and no magnetic order. Since d orbitals compose chemical bonding, their wave function has a direct information of their crystal symmetry. In addition to this, we can get another advantage in $5d$ electron system which is described as follows.

Usually, $3d$ orbital systems have a well known characteristics as strongly correlated electron system which arise from electron-electron coulomb interaction. Mott insulator or high-temperature cuprate superconductor and so on are the typical examples. However in $5d$ orbital systems it will diminish because of enhancement of the orbital broadening. Therefore we tend to take it that $5d$ electron system has no interesting physical phenomenons. Actually, it is not always true because of the existence of strong spin-orbit interaction. Fortunately, electron-electron coulomb interaction is weak but spin-orbit interaction is strong is an optimal situation from the standpoint of parity mixing. This is because strong interelctron coulomb interaction breaks the energy levels of the wave modes between spin singlet and spin triplet states. In contrast weak interelectron interaction move them closer. Therefore, realization of the mixing is anticipated in $5d$ with strong spin-orbit interaction. In that sense, $5d$ electron system has a priority to understand the pure effect of SOC into superconductivity. Incidentally, $3d$ electron system is applicable to L-S coupling whereas $5d$ is j-j coupling from above discussion.

	$3d$	$5d$
Interelectron coulomb interaction	strong	weak
Spin-orbit interaction	weak	strong
Electronic scheme	L-S coupling	j-j coupling

Table 1.3: Brief categorization for d electron system

1.10.2 $Li_2(Pd, Pt)_3B$

Figure 1.5 gives crystal structure of $Li_2(Pd, Pt)_3B$ which are recent discovered superconductors [38]. Left and right figures show the unit cell and distorted octahedrons [11]. Each atom of this crystal has no inversion symmetry in all directions and the structure remains unchanged in low temperature [36].

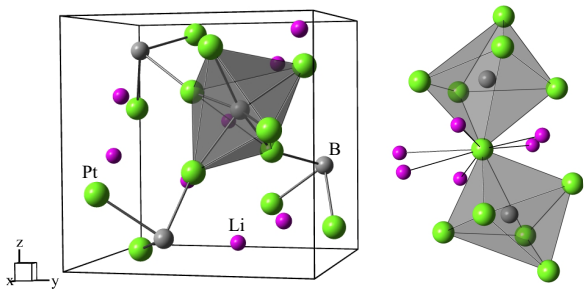

Figure 1.5: Crystal structure of $Li_2(Pd, Pt)_3B$ with broken inversion symmetry.

These T_c are about 7 K, 2.7 K, respectively. It is reported from NMR [28, 29], penetration depth [44] and specific heat [35] measurement that these superconducting properties are different.

In NMR, the spin-lattice relaxation rate $1/T_1$ and Knight shift measurements probed by ^{11}B NMR prove that the superconducting gap symmetry and spin symmetry are isotropic (*s*-wave) and spin singlet state in Li_2Pd_3B, while anisotropic (line node) and spin triplet state in Li_2Pt_3B. **Figure** 1.6 (a) shows the temperature dependence of $1/T_1$ in $Li_2(Pd, Pt)_3B$. In Li_2Pd_3B, it can be seen the enhancement of $1/T_1$ just below T_c, which is well known characteristic as coherence peak with conventional *s*-wave gap. However in Li_2Pt_3B, there is no coherence peak and $1/T_1 \sim T^3$ behavior exists in the lower temperature, which indicates the existence of line node gap structure.

Figure 1.6 (b) shows the temperature dependence of Knight shift (^{11}K). In Li_2Pd_3B with isotropic gap, ^{11}K changes below T_c. It means the decrease of spin susceptibility by forming the spin singlet paring. In Li_2Pt_3B with anisotropic gap, it remains unchanged. These results indicate that the spin singlet state is dominant in Li_2Pd_3B while, the spin triplet state is dominant in Li_2Pt_3B since spin angular momentum of Cooper pairs will be killed by the spin singlet pairing whereas

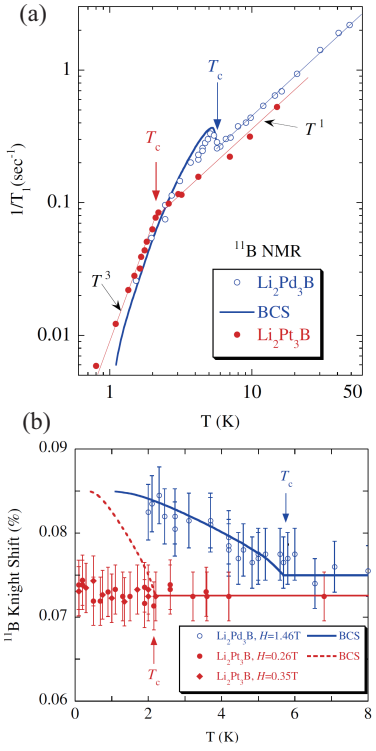

Figure 1.6: Temperature dependence of spin-lattice relaxation rate ($1/T_1$) in $Li_2(Pd, Pt)_3B$.

it will survive in the spin triplet state.

Penetration depth [44] and specific heat measurements [35] also report that Li_2Pt_3B has anisotropic gap structure. As reported by Yuan, *et al.* [44], the linear temperature dependence of penetration depth (λ) was found in Li_2Pt_3B while in Li_2Pd_3B, λ decreases exponentially. It indicates that Li_2Pd_3B and Li_2Pt_3B have isotropic (*s*-wave) and anisotropic (line node) gap structure, respectively. Furthermore, specific heat measurement [35] supports Li_2Pt_3B has line nodes. They are consistent with the NMR measurements.

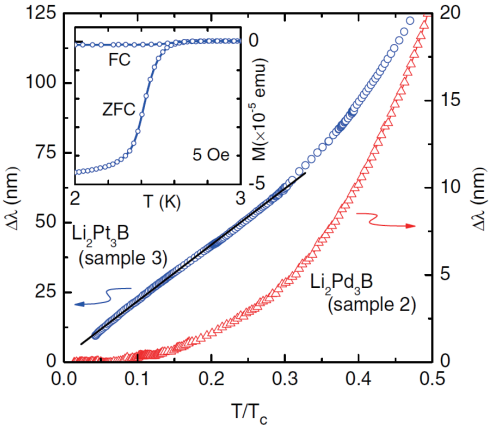

Figure 1.7: Temperature dependence of penetration depth in $Li_2(Pd, Pt)_3B$.

What is the origin of the two different superconducting properties despite their same crystal system? The answer is believed as their strength of SOC originated from Pd or Pt. Namely, it means that strong SOC induces the novel spin triplet state for Li_2Pt_3B. If this prediction is correct, we can control their superconducting symmetry by tunning SOC. Incidentally, it is reported that these compounds are weakly electronic correlated system [40, 43] and thus the mixing is anticipated.

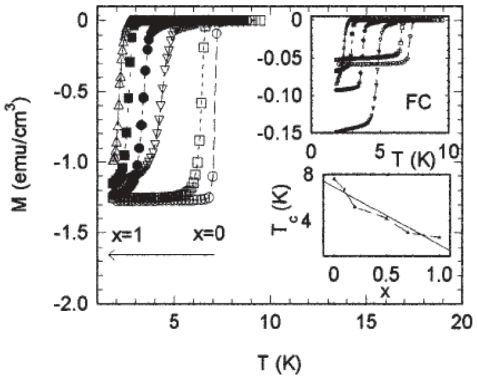

Figure 1.8: Phase diagram from Badica, *et al.* [6].

Mixed crystal system $Li_2(Pd_{1-x}Pt_x)_3B$ also shows the superconductivity, which was reported by Badica, *et al.* [6]. By their report, it is confirmed that the fundamental structure remains unchanged for $x = 0 - 1$. Also, their bulk superconducting properties are retained while the T_c decreases smoothly with increasing x. This compounds arouse our interest since the control of Cooper pair's symmetry is possible by regulation of their spin-orbit interaction. Therefore, it is ideal material to confirm the anticipation.

However, the superconducting properties have not been established in spite of the strong interests. Therefore, NMR investigations on $Li_2(Pd_{1-x}Pt_x)_3B$ were conducted in this doctoral dissertation.

Finally, I want to demonstrate the significance of the study. (1) Occurrence of unconventional superconductivity in weak electronic correlated system on $Li_2(Pd, Pt)_3B$ is a novel phenomenon which is derived from spin-orbit interaction and has an advantage to discuss just spin-orbit coupling effect into superconducting pairing symmetry. To clarify the origin, $Li_2(Pd_{1-x}Pt_x)_3B$ is the strongest tool. (2) Study of the role of spin-orbit interaction in superconductivity is poorer compared to the other fields such as magnetism. There is room for further research into superconductivity.

From the research, I wish to produce basic idea of NCS superconductor.

Chapter 2

Sample Preparation

In this chapter, actual procedures and details of sample preparation will be presented. The crystalline characteristics were investigated by X-ray diffraction and the superconducting properties were also checked by SQUID. The results will be remarked as well

2.1 Sample Synthesis

The sample synthesis of $Li_2(Pd_{1-x}Pt_x)_3B$ was conducted using arc melting method. In the method we can get high temperature environment immediately by electric discharge. It is suitable to make $Li_2(Pd_{1-x}Pt_x)_3B$ because the melting points of Pt, Pd, B are comparatively high except Li, which are about 2000 °C. Because of small heating area, we will get a small sample. Moreover, we have to shot several times after turning over the samples because of homogenization.

The sample was synthesized by two step arc melting method. In the first step $(Pd_{1-x}Pt_x)_3B$ are prepared using Pt(99.999%), Pd(99.95%), B(99.8%). The weight losses

after the melting are negligible. Actually, it have been checked that the ratio of Pt and Pd remains unchanged from energy dispersive X-ray spectroscopy (EDX).

In the next step, Li(99%) was mixed. Increased Li were prepared considering the evaporation of Li. It is found that the synthesis becomes more difficult as x comes up to $x = 1$.

Figure 2.1: Arc furnace for synthesis of $Li_2(Pd_{1-x}Pt_x)_3B$

2.2 X-ray Diffraction

The synthesized polycrystalline samples are checked by powder X-ray diffraction. The principles of X-ray diffraction has been described in any textbooks. Therefore, it is not remarked in this thesis.

Figure 2.2 shows the result of the synthesis in which Li was increased by 5%. For $x = 0 - 0.8$, the diffraction peak corresponds to that of the $Li_2(Pd_{1-x}Pt_x)_3B$ phase. However, it was found that impurity phase appears for $x = 0.84, 0.9, 1$, which have been identified as Li_1Pt_3B phase. Simulation of the diffraction pattern of Li_2Pt_3B and Li_1Pt_3B are represented in **Fig**. 2.3, which explains every peak in $x = 0.84, 0.9, 1$ with impurity, Li_1Pt_3B.

The difficulty indicates that the impurity appears because of some defects of Li during the synthesis. To improve this, $10 - 30\%$ increased Li was used for $x = 0.84, 0.9, 1$. As a result, single phase of $Li_2(Pd_{1-x}Pt_x)_3B$ are obtained. The Rietveld analysis was conducted to see the crystal transformations with increasing x. The result will be remarked in **Discussion**.

The superconductivity was checked by SQUID. The superconducting volume is consistent with the report by Badica *et al*. The sample synthesis was completed. Next, NMR measurement was conducted to see electronic information.

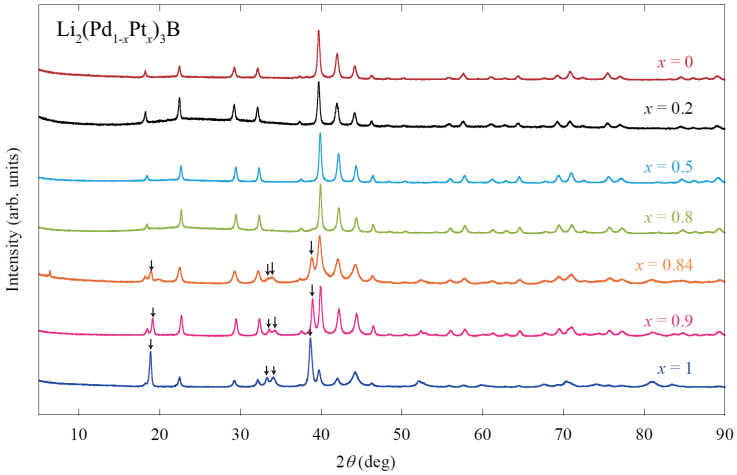

Figure 2.2: Results of X-ray diffraction in $Li_2(Pd_{1-x}Pt_x)_3B$ where Li have been increased by 5%.

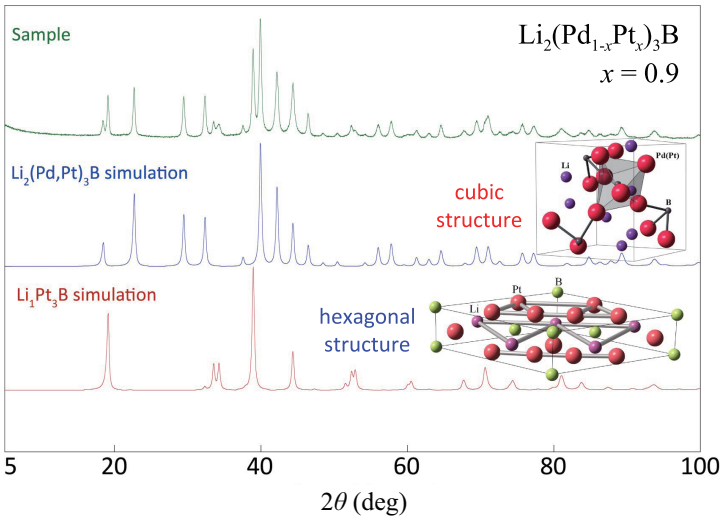

Figure 2.3: Comparison of the diffractive result for $Li_2(Pd_{0.1}Pt_{0.9})_3B$ with simulation of Li_2Pt_3B and Li_1Pt_3B phases.

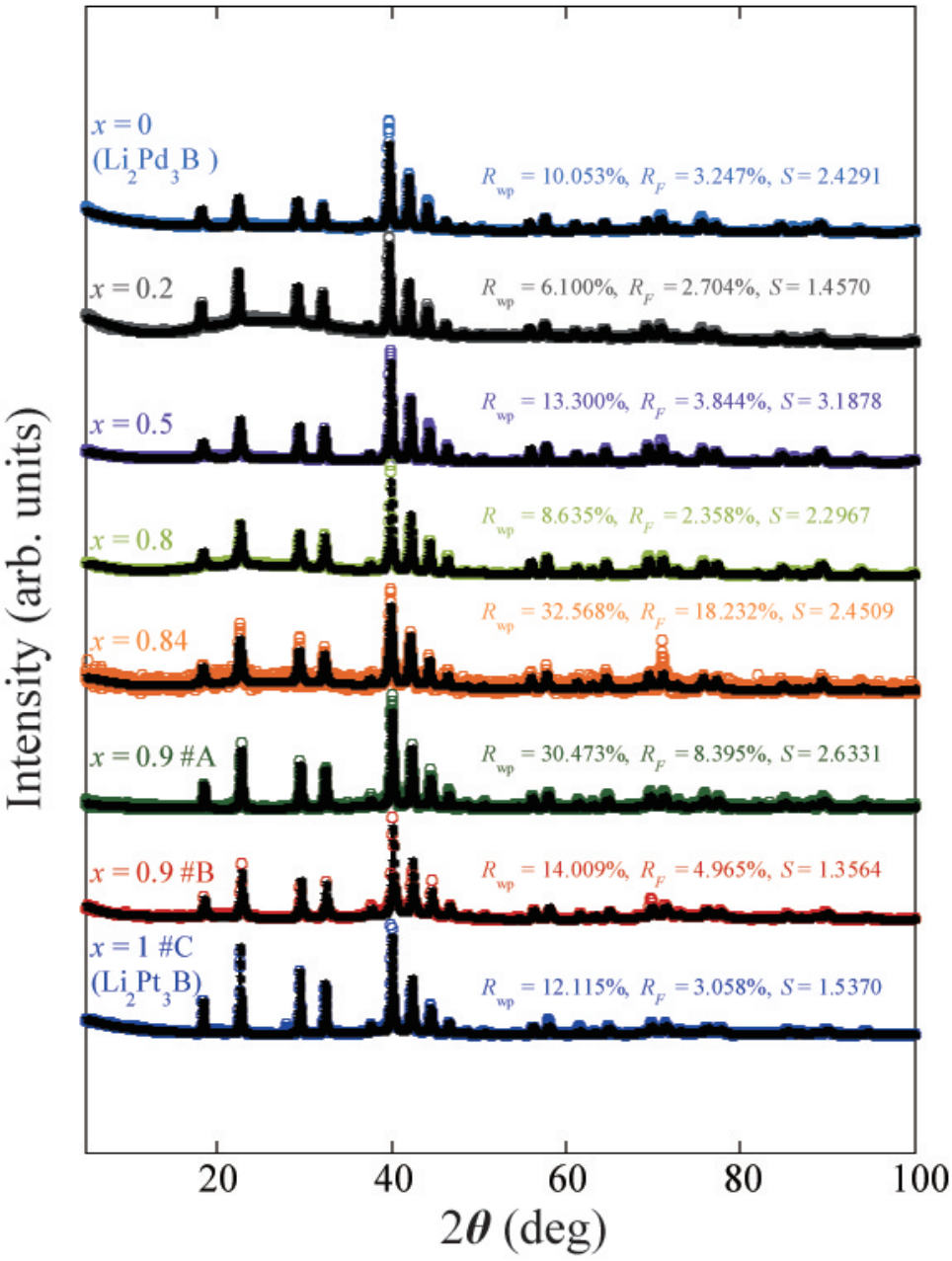

Figure 2.4: Final results of XRD. These samples were used for NMR investigation.

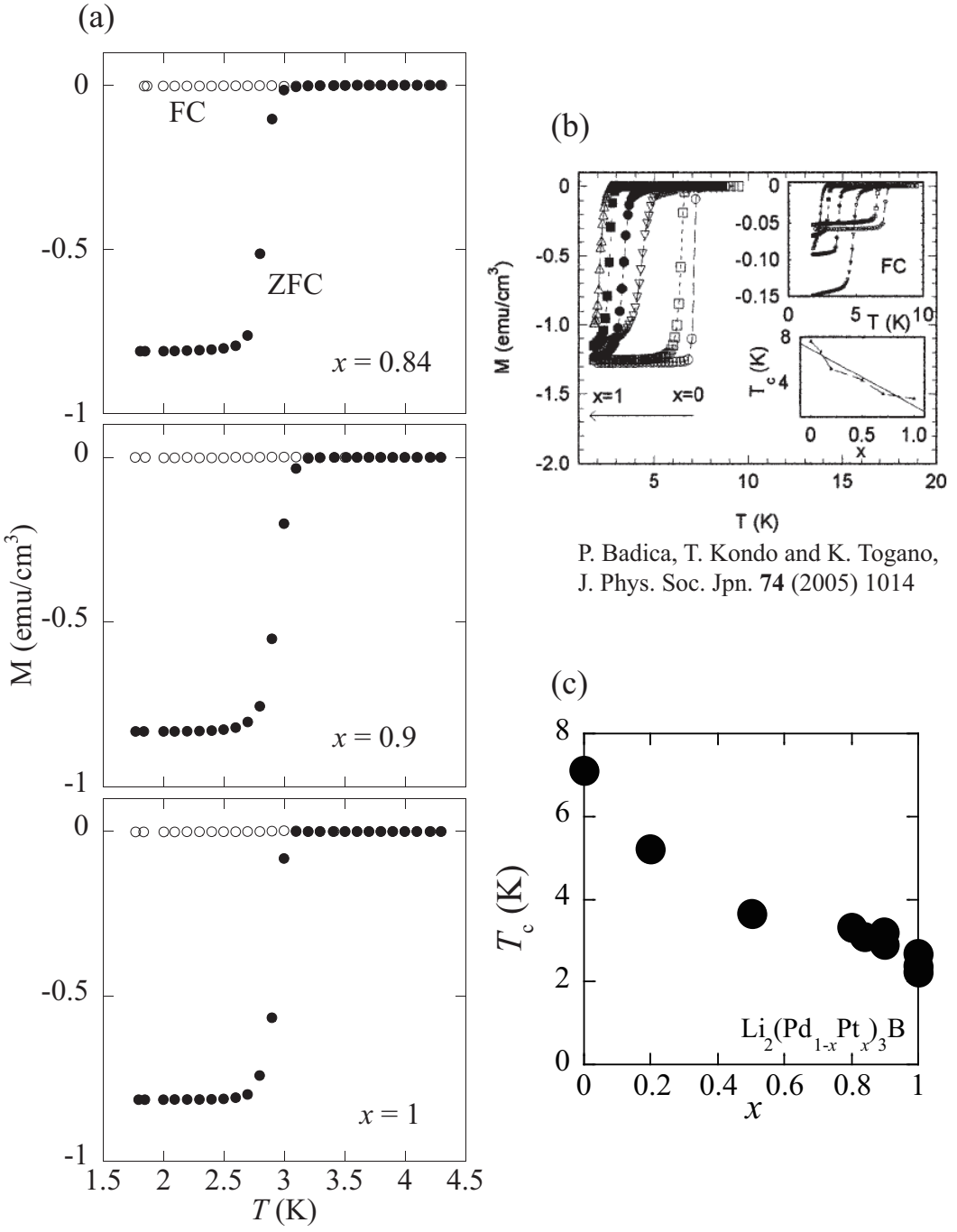

Figure 2.5: (a) Temperature dependence of magnetization in the synthesized $Li_2(Pd_{1-x}Pt_x)_3B$, $x = 0.84, 0.9, 1$. (b) Temperature dependence of magnetization from the report by Badica, *et al* [6]. (c) Phase diagram of $Li_2(Pd_{1-x}Pt_x)_3B$.

Chapter 3

Measurements

In this study, nuclear magnetic resonance (NMR) method was conducted for the investigation. The brief principle will be remarked as follows [3, 33].

3.1 Nuclear Magnetic Resonance (NMR)

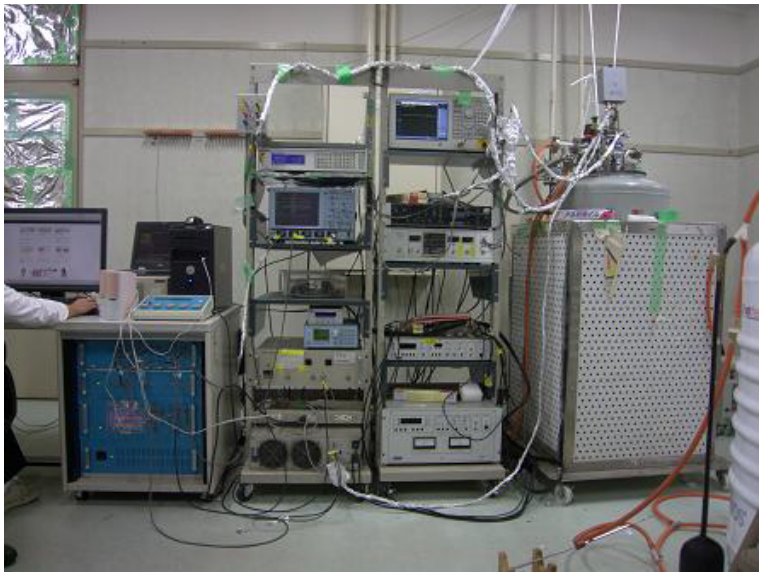

Figure 3.1: Picture of NMR system

3.1.1 Hyperfine Interaction

In NMR, we can take electron informations through nuclear-electron interactions. Nuclear and electronic magnetic coupling is named as hyperfine interaction. It can be envisioned as follows,

***s*-states: Contact interaction**

$$\mathcal{H}_{\mathrm{F}} = \frac{8\pi}{3}\gamma_e\gamma_n\hbar^2 \boldsymbol{I} \bullet \boldsymbol{S}\delta(\boldsymbol{r}) \tag{3.1}$$

Because of δ function, the above interaction contributes only to s-states having their existence at $r = 0$.

Non-s-states: Dipole interaction, Orbital term

$$\mathcal{H}_{\rm dip} = \frac{\gamma_e \gamma_n \hbar^2}{r^3}\left[\frac{3(\boldsymbol{I}\bullet\boldsymbol{r})(\boldsymbol{S}\bullet\boldsymbol{r})}{r^2} - \boldsymbol{I}\bullet\boldsymbol{S}\right] \tag{3.2}$$

$$\mathcal{H}_{\rm orb} = \gamma_e \gamma_n \hbar^2 \frac{\boldsymbol{I}\bullet\boldsymbol{l}}{r^3} \tag{3.3}$$

The former is dipole interaction and latter is interaction between electronic orbital and nuclear spin, respectively. It will contribute to non-s-state since for s-states, they will vanish. It is noted that when orbital radius is large, their contribution will weaken compared to $H_{\rm F}$ because of $\left\langle 1/r^3 \right\rangle$ term.

3.1.2 Interaction between Nuclear Spin and External Magnetic Field

When an external magnetic field are applied, a nuclear magnetic moment will couple with it through Zeeman interaction. Therefore, the interaction under magnetic field $\boldsymbol{H}_0$ is,

$$\mathcal{H}_Z = -\boldsymbol{\mu}_N \bullet \boldsymbol{H}_0 \tag{3.4}$$
$$= -\gamma\hbar \boldsymbol{I}_N \bullet \boldsymbol{H}_0. \tag{3.5}$$

Taking the field to be H_0 along the z-direction, the energy eigenvalue $\langle H_Z \rangle = E_m$ is envisioned as,

$$E_m = -\gamma\hbar H_0 m. \tag{3.6}$$

Usually, the energy split is about $1 \sim 100$ MHz. Therefore, NMR is suitable to investigate low temperature electronic states.

3.1.3 Spin Lattice Relaxation Rate $(1/T_1)$

In the external field, equation of magnetic motion is described as Bloch function using total magnetic moment $\boldsymbol{M} = \sum_i \boldsymbol{\mu}_i$,

$$\frac{dM_z}{dt} = \gamma(\boldsymbol{M}\times\boldsymbol{H})_z + \frac{M_0 - M_z}{T_1} \tag{3.7}$$
$$\frac{dM_{x,y}}{dt} = \gamma(\boldsymbol{M}\times\boldsymbol{H})_{x,y} - \frac{M_{x,y}}{T_2} \tag{3.8}$$

where T_1, T_2 are named as spin-lattice and spin-spin relaxation time. We focus on T_1 in the following discussion. Since the $\boldsymbol{H}$ = (0, 0, H_0), **Equation** (3.7) becomes

$$\frac{dM_z}{dt} = \frac{M_0 - M_z}{T_1}. \tag{3.9}$$

It can be seen $M_z = M_0$ in the static state because $dM_z/dt = 0$.

In the dynamic state,

$$M_z = M_0(1 - e^{-t/T_1}) \tag{3.10}$$

assuming the initial state as $M_z(0) = 0$.

By applying the external field, the magnetic moment will move to the direction along with z axis. However, soon after knocking down the magnetization by irradiation of oscillating magnetic field (rf pulse), M_z becomes zero. Then, M_z recovers exponentially to the equilibrium state using a time named as spin-lattice relaxation time T_1. By measurement of T_1, we can obtain electronic dynamic informations since M_z recovers by interacting with electrons. Incidentally the equilibrium magnetization as having frequency w_0 has precessional motion in the x-y plane. Therefore, only when the frequency of the oscillating magnetic field is $w = w_0$, the resonance occurs.

Formally, the spin-lattice relaxation rate can be expressed as

$$\frac{1}{T_1} = \frac{1}{2}\frac{\sum_{n,m} W_{m,n}(E_m - E_n)^2}{\sum_n E_n^2} \tag{3.11}$$

where $W_{m,n}$ is a transition probability through hyperfine interaction from Fermi's Golden Rule

$$\begin{aligned} W_{m,n} &= \frac{2\pi}{\hbar}\left|\left\langle m\middle|\mathcal{H}_{\rm hyp}\middle|n\right\rangle\right|^2 \rho_m(E_m) && (3.12)\\ \mathcal{H}_{\rm hyp} &= \mathcal{H}_{\rm F}, \mathcal{H}_{\rm dip}, \mathcal{H}_{\rm orb}, \ldots && (3.13)\\ \rho_m(E_m) &= N(E_m)N(E_n)f(E_m)\{1 - f(E_n)\} && (3.14)\\ &\simeq N(E_f)^2 k_{\rm B}T && (3.15) \end{aligned}$$

$N(E)$ is a density of state and $f(E)$ is a Fermi distribution function.

It is found that $1/T_1$ is proportional to $N(E_f)^2$. Since $1/T_1$ gives a information of $N(E_f)$, we can determine electronic system through $1/T_1$ as a function of T. As a result, $1/T_1$ has a following relations.

In normal state,

$$\left(\frac{1}{T_1}\right)^{N.S.} \sim \begin{cases} T & : \text{metallic system} \\ \dfrac{T}{(T - T_c)^{\alpha}} & : \text{magnetic system} \end{cases} \tag{3.16}$$

In superconducting state,

$$\left(\frac{1}{T_1}\right)^{SC.S.} \sim \begin{cases} \exp\left(-\dfrac{\Delta}{k_{\rm B}T_{\rm c}}\right) & : \text{fullgap} \\ T^3 & : \text{linenode} \\ T^5 & : \text{pointnode} \\ T & : \text{gapless.} \end{cases} \tag{3.17}$$

Usually, we judge superconducting gap symmetry by the power of T. Especially in BCS superconductor, the $1/T_1$ has a coherence peak just below $T_{\rm c}$.

3.1.4 Knight Shift

In normal state in metal and magnetic material, conduction electrons or localized electrons makes magnetization at nuclear position which is induced by external field. Therefore, the nuclear feels another magnetic field ΔH in addition to the external field H_0. The shift is named as Knight shift which can be defined as

$$K = \frac{\Delta H}{H_0} \tag{3.18}$$

where ΔH originates from the hyperfine interaction. The expected values of the hyperfine magnetic field $\Delta H_{\rm hf}$ are given as follows

$$\langle \boldsymbol{H}_{\rm orb}\rangle_i = -\gamma_e\hbar\langle \boldsymbol{l}\rangle_i \left\langle \psi^* \left| \frac{1}{r^3} \right| \psi \right\rangle \tag{3.19}$$

$$\left\langle \boldsymbol{H}_{\rm dip}\right\rangle_i = \gamma_e\hbar \left\langle \psi^* \left| \frac{\langle \boldsymbol{S}\rangle}{r^3} - 3\frac{(\langle \boldsymbol{S}\rangle \bullet \boldsymbol{r})\boldsymbol{r}}{r^5} \right| \psi \right\rangle_i \tag{3.20}$$

$$\langle \boldsymbol{H}_{\rm F}\rangle_i = -\frac{8\pi}{3}\gamma_e\hbar\langle \boldsymbol{S}\rangle_i |\psi(0)|^2 \tag{3.21}$$

$$\left\langle \boldsymbol{H}_{\rm cp}\right\rangle_i = -\frac{8\pi}{3}\gamma_e\hbar\langle \boldsymbol{S}\rangle_i \sum_j \left(|\psi_j(0)|^2_\uparrow - |\psi_j(0)|^2_\downarrow\right). \tag{3.22}$$

We have following relations

$$-\gamma_e\hbar\langle \boldsymbol{S}\rangle_i = \chi^i_s H^i_0 \tag{3.23}$$

$$-\gamma_e\hbar\langle \boldsymbol{l}\rangle_i = \chi^i_{\rm vv} H^i_0 \tag{3.24}$$

where χ^i_s is a spin susceptibility and $\chi^i_{\rm vv}$ is a Van-Vleck susceptibility along with i-axis. Therefore, we can display the spin susceptibility in the equations as below,

$$\langle \boldsymbol{H}_{\rm orb}\rangle_i = \chi^i_{\rm vv}\left\langle \psi^* \left| \frac{1}{r^3} \right| \psi \right\rangle H^i_0 \tag{3.25}$$

$$\langle \boldsymbol{H}_{\rm dip}\rangle_i = -\left\langle \psi^* \left| \frac{\chi^i_s}{r^3} - 3\frac{\sum_i \chi^i_s x_i}{r^5} x_i \right| \psi \right\rangle H^i_0 \tag{3.26}$$

$$\langle \boldsymbol{H}_{\rm F}\rangle_i = \frac{8\pi}{3}\chi^i_s|\psi(0)|^2 H^i_0 \tag{3.27}$$

$$\langle \boldsymbol{H}_{\rm cp}\rangle_i = \frac{8\pi}{3}\chi^i_s \sum_j \left(|\psi_j(0)|^2_\uparrow - |\psi_j(0)|^2_\downarrow\right) H^i_0. \tag{3.28}$$

From **Equation** (3.18), K will be

$$\langle \boldsymbol{K}_{\rm orb}\rangle_i = \chi^i_{\rm vv}\left\langle \psi^* \left| \frac{1}{r^3} \right| \psi \right\rangle \tag{3.29}$$

$$\langle \boldsymbol{K}_{\rm dip}\rangle_i = -\left\langle \psi^* \left| \frac{\chi^i_s}{r^3} - 3\frac{\sum_i \chi^i_s x_i}{r^5} x_i \right| \psi \right\rangle \tag{3.30}$$

$$\langle \boldsymbol{K}_{\rm F}\rangle_i = \frac{8\pi}{3}\chi^i_s|\psi(0)|^2 \tag{3.31}$$

$$\langle \boldsymbol{K}_{\rm cp}\rangle_i = \frac{8\pi}{3}\chi^i_s \sum_j \left(|\psi_j(0)|^2_\uparrow - |\psi_j(0)|^2_\downarrow\right) \tag{3.32}$$

where $\langle \boldsymbol{K}_{\rm F}\rangle_i$, $\langle \boldsymbol{K}_{\rm cp}\rangle_i$ contribute to s-state and non-s-state such as p, d, f,...states, respectively. Incidentally, $K_s \sim \chi_s$ is proportional to $N(E_f)$.

The Knight shift is convenient tool to judge superconducting spin symmetry (singlet/triplet) since ${}^1\chi^i_s$ decreases while ${}^3\chi^i_s$ remains unchanged below T_c where ${}^1\chi^i_s$ and ${}^3\chi^i_s$ give the susceptibility of spin singlet ($S = 0$) and spin triplet ($S = 1$) states, respectively.

3.2 Condition of NMR measurement

Figure 3.2: Picture of ^{3}He-^{4}He dilution refrigerator

NMR measurements were conducted under magnetic field below $H \leq 0.44$ T in order to minimize the reduction of T_c by the H. The NMR spectrum were obtained by fast Fourier transform of the spin echo taken at the fixed H. The spin-lattice relaxation rate $1/T_1$ was measured for ^{11}B, ^{195}Pt and ^{7}Li, and determined by a good fit of the recovery of the nuclear magnetization to a single exponential function. For the alloyed samples, ^{195}Pt Knight shift was measured, since it is much larger than that of ^{11}B or ^{7}Li and provides higher accuracy for broadened spectra due to alloying. Measurements below 1.4K were carried out with a ^{3}He-^{4}He dilution refrigerator.

3.3 ^{195}Pt NMR spectrum

NMR spectra for ^{195}Pt nucleus are presented in **Fig**. 3.3 where Li_2Pt_3B #A is referred from [29] and $Li_2(Pd_{0.1}\ Pt_{0.9})_3B$ #A and $Li_2(Pd_{0.1}\ Pt_{0.9})_3B$ #B are the same composition but have different T_c (#A: 2.9 K, #B: 3.2 K). It seems that the #B is better sample than #A. All the spectra show a single peak which is consistent with XRD analysis. It has been confirmed that ^{195}Pt NMR spectrum for Li_1Pt_3B has the lower resonance frequency. Therefore, we can identify the sample by NMR as well as XRD.

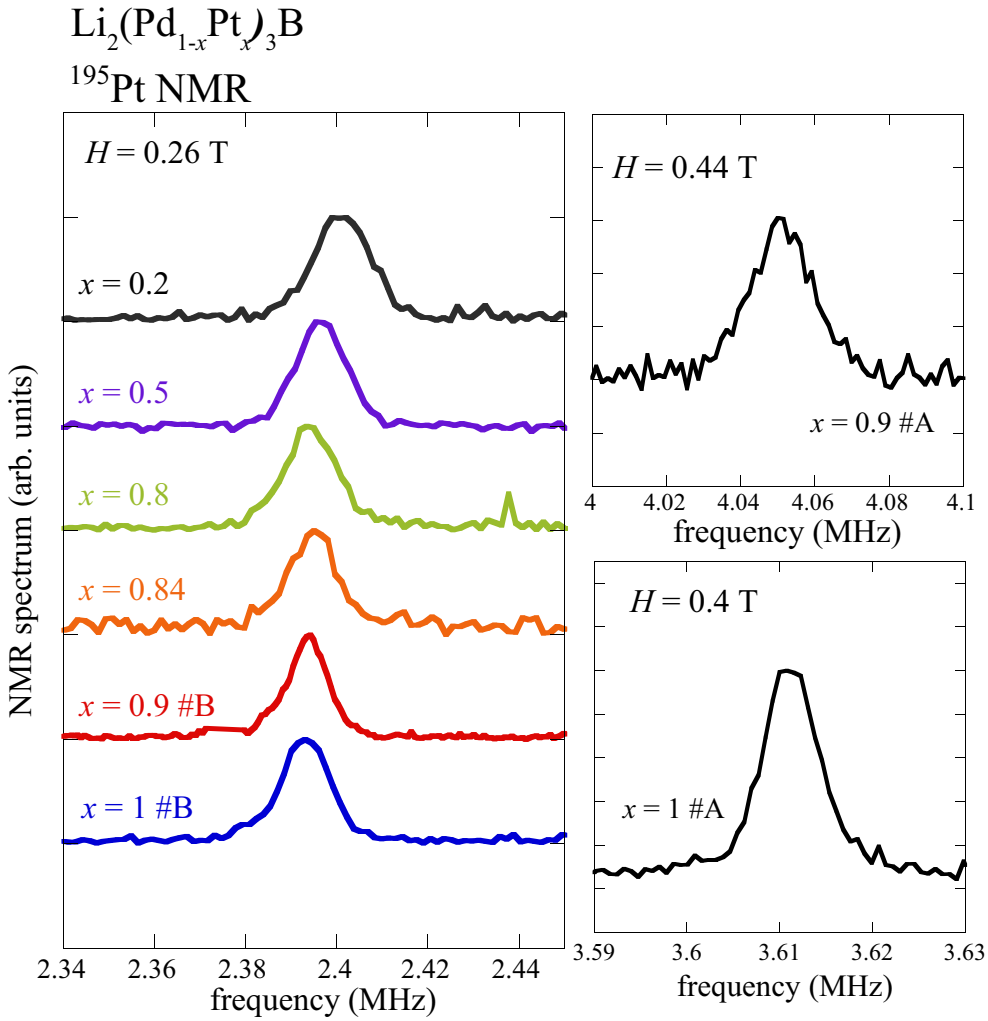

Figure 3.3: NMR spectra for ^{195} Pt nucleus

Chapter 4

Results

In this Chapter, results of NMR measurement and Rietveld analysis will be shown.

4.1 ^{11}B NMR

^{11}B nucleus, which is arranged in the center of the octahedron, is useful probe to see the electronic transformation for $Li_2(Pd_{1-x}Pt_x)_3B$. Since it does not change the composition ratio with increasing x, we can make a constant judge to each sample. However, temperature dependence of ^{11}Knight shift, ^{11}K have not been conducted. Since ^{11}K is very tiny from **Fig**. 1.6 (b), we need quite a lot of accuracy. Hence, we can not adopt the measurement because mixed crystal make the spectrum spread.

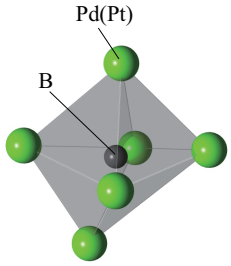

Figure 4.1: Nearest neighborhoods around ^{11}B

Temperature dependence of spin lattice relaxation rate, $^{11}1/T_1$ is shown in **Fig**. 4.2. For $x = 0, 0.2, 0.5, 0.8$, there is a coherence peak just below T_c. This feature indicates the superconducting gap has isotropic s-wave structure with conventional BCS superconductor. The solid lines on the plots for $x = 0$–0.8 are fitting curves assumed as BSC superconductor. Considering that external field suppresses extent of the jump, the magnitude of gap is almost constant with increasing x, meaning that the superconducting gap symmetry almost remains unchanged for $x = 0 - 0.8$ (see Table 4.1).

composition, x	$2\Delta_0/k_BT_c$
0	3.4
0.2	3.12
0.5	3.5
0.8	2.93

Table 4.1: Result of BSC fitting for $x = 0, 0.2, 0.5, 0.8$

However with increasing x further, it was found that the coherence peak disappears for $x = 0.9, 1$. Furthermore, the $^{11}1/T_1$ is proportional to T^3 as temperature decreases below T_c. This feature is unconventional superconducting behavior with line node.

From $^{11}1/T_1$ measurement, it was found that the superconducting gap structure suddenly changes around $x = 0.8 - 0.9$.

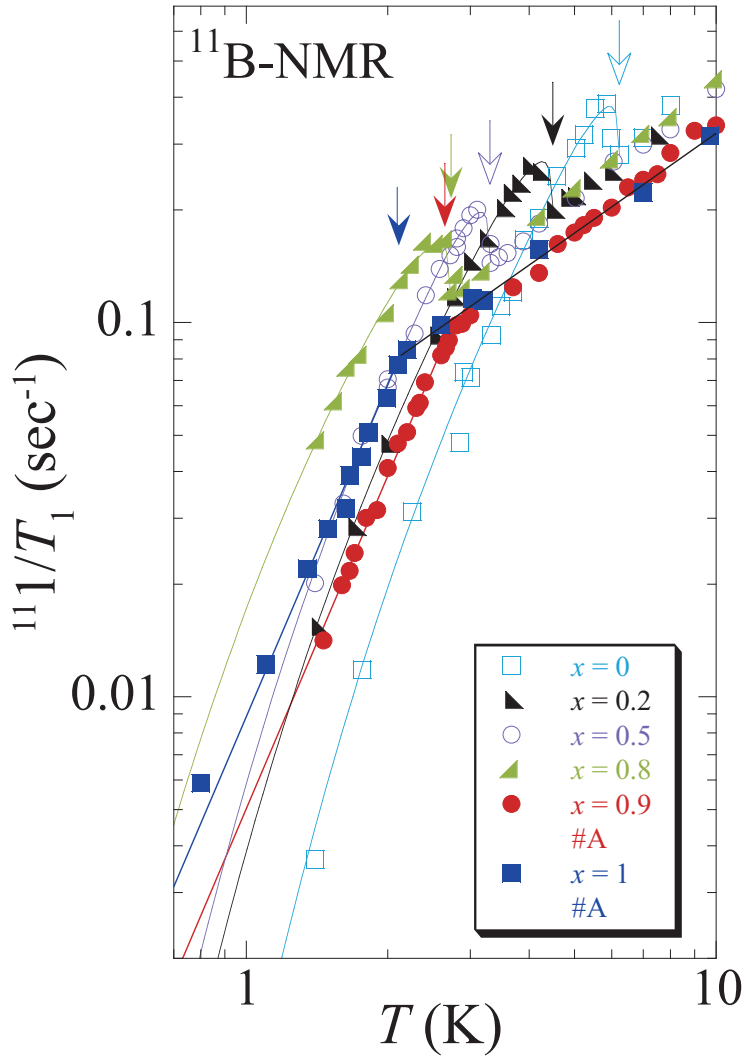

Figure 4.2: $^{11}(1/T_1T)$ in $Li_2(Pd_{1-x}Pt_x)_3B$ probed by ^{11}B NMR. The solid lines below T_c for $x = 0, 0.2, 0.5, 0.8$ are fitting by BCS theory and for $x = 0.9, 1$ shows a line which is proportional to T^3.

4.2 ^{195}Pt NMR

In summary of $^{11}1/T_1$ measurements and our expectations, investigation of electronic state around ^{195}Pt nucleus for $x = 0.8 - 1$ is meaningful. First, superconducting symmetry will be in the spotlight. The normal state properties are discussed after that.

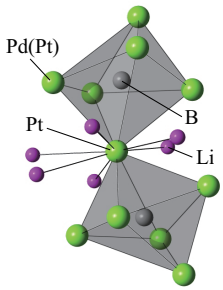

Figure 4.3: Neighborhoods around ^{195}Pt

4.2.1 spin lattice relaxation rate -superconducting state-

Figure 4.4 (a) gives the temperature dependence of $^{195}1/T_1$ for $x = 0.84, 0.9, 1$. For $x = 0.9, 1$, the behavior is the same with $^{11}1/T_1$. In short, $^{195}1/T_1$ has no coherence peak at T_c and decreases with $^{195}1/T_1 \sim T^3$. Though for $x = 0.84$, the behavior is a little different. There is a tiny coherence peak at T_c. It may arise from the mixing behavior of s-wave gap and line node gap.

For $x = 0.9$, low temperature behavior below 1K has been investigated, **Fig**. 4.4 (b). At very low temperature, $^{195}1/T_1$ becomes to be in proportion to T, which is due to impurity scattering in case of a nodal superconductor. This is a proof of existence of nodes because quasiparticles scattered into nodes bring about a finite density of state in the superconducting gap, whereas in a conventional nodeless superconductivity, they do not.

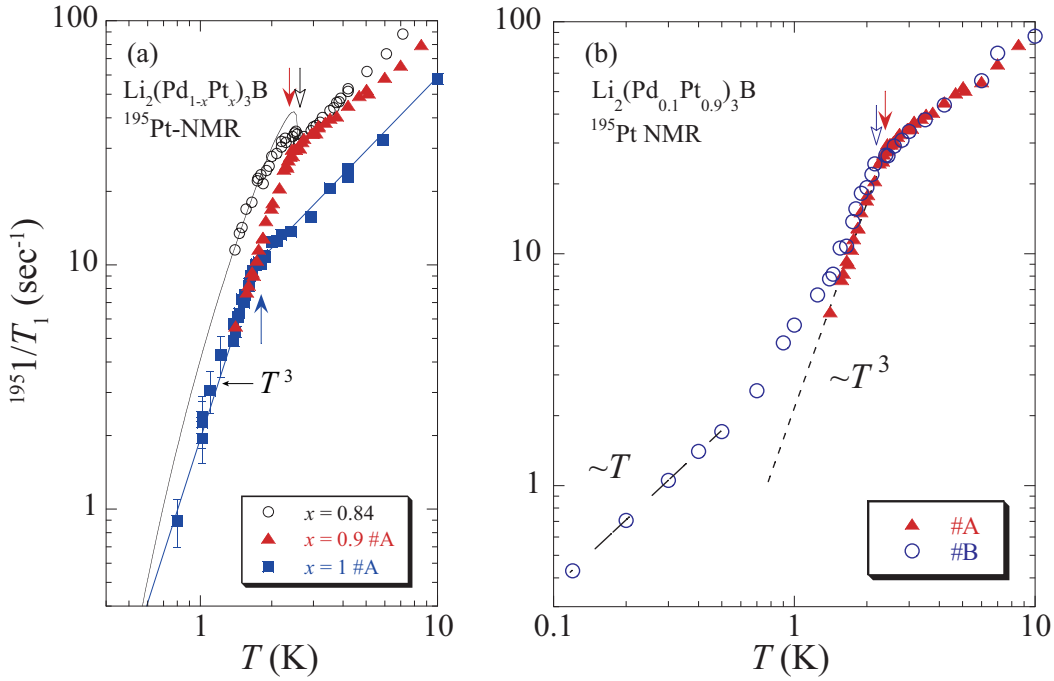

Figure 4.4: (a) Temperature dependence of $^{195}1/T_1$ for $x = 0.84, 0.9, 1$. (b) Low temperature behavior of $^{195}1/T_1$ for $x = 0.9$.

Incidentally, the residual density of state (RDOS) is estimated to be 60% for effective DOS, that is comparatively large (see **Fig**. 4.5). The reason is due to existence of

energy bands near E_F despite the gap being completely opened. It is expected that the residual energy bands were made due to development of impurities and/or intrinsic nodal structure that run across the Fermi surface.

As a result, it is unnatural to take impurity was developed because full width of half maximum (FWHM) of ^{195}Pt spectrum has no enhancement. The expansion of FWHM would be observed if the sample purity became worse around $x \sim 0.9$. Actually, it has a dome structure with a summit at $x = 0.5$ which is consistent behavior with previous report of residual resistivity versus x (**Fig**. 4.6, [32]). From that reason, to take nodal structure have been developed for $x \sim 0.8$ is the most reasonable interpretation.

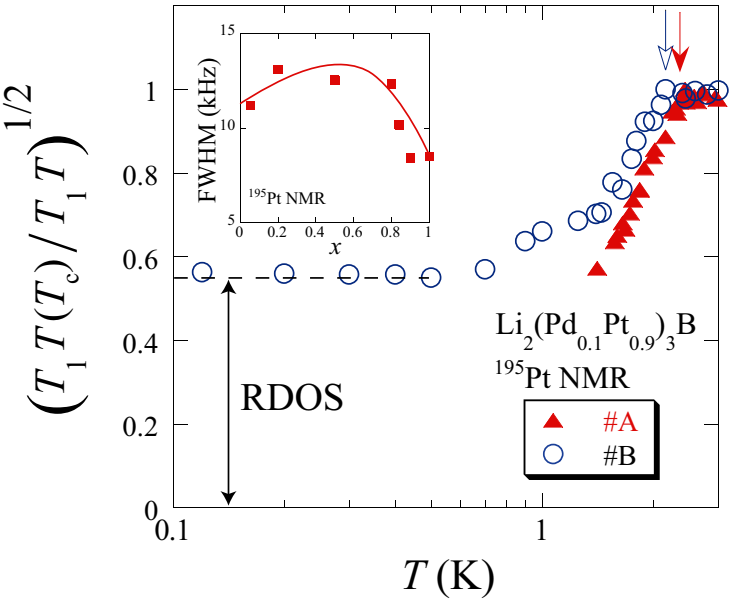

Figure 4.5: Temperature dependence of $(^{195}1/T_1T)^{1/2}$ for $x = 0.9$, which is normalized by T_c. Inset shows FWHM of ^{195}Pt NMR spectrum.

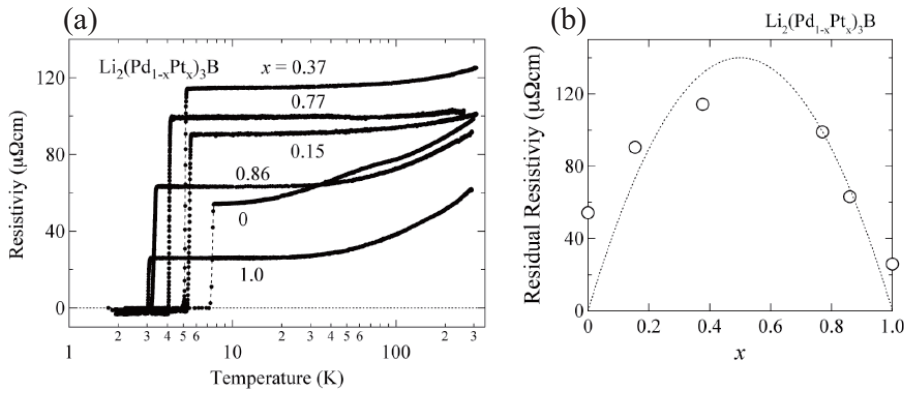

Figure 4.6: (a) Temperature dependence of resistivity on $Li_2(Pd_{1-x}Pt_x)_3B$. (b) Residual resistivity as a function of x. They are referred from [32]

4.2.2 Knight shift -superconducting state-

To see whether the spin state of Cooper pairs is in the spin singlet state or in the spin triplet state, spin susceptibility measurement χ_s via Knight shift is the most effective probe because χ_s in the spin singlet state will vanish at $T = 0$, while in the spin triplet state it will remain unchanged.

The temperature dependence of ^{195}Pt Knight shift (^{195}K) for $x = 0.2, 0.5, 0.8, 0.84, 0.9, 1$ is shown in **Fig**. 4.7. ^{195}K for $x = 0.2, 0.5, 0.8$ decreases below T_c. However for $x = 0.9, 1$, it remains unchanged across T_c. The Knight shift for $x = 0.84$ shows a small reduction below T_c.

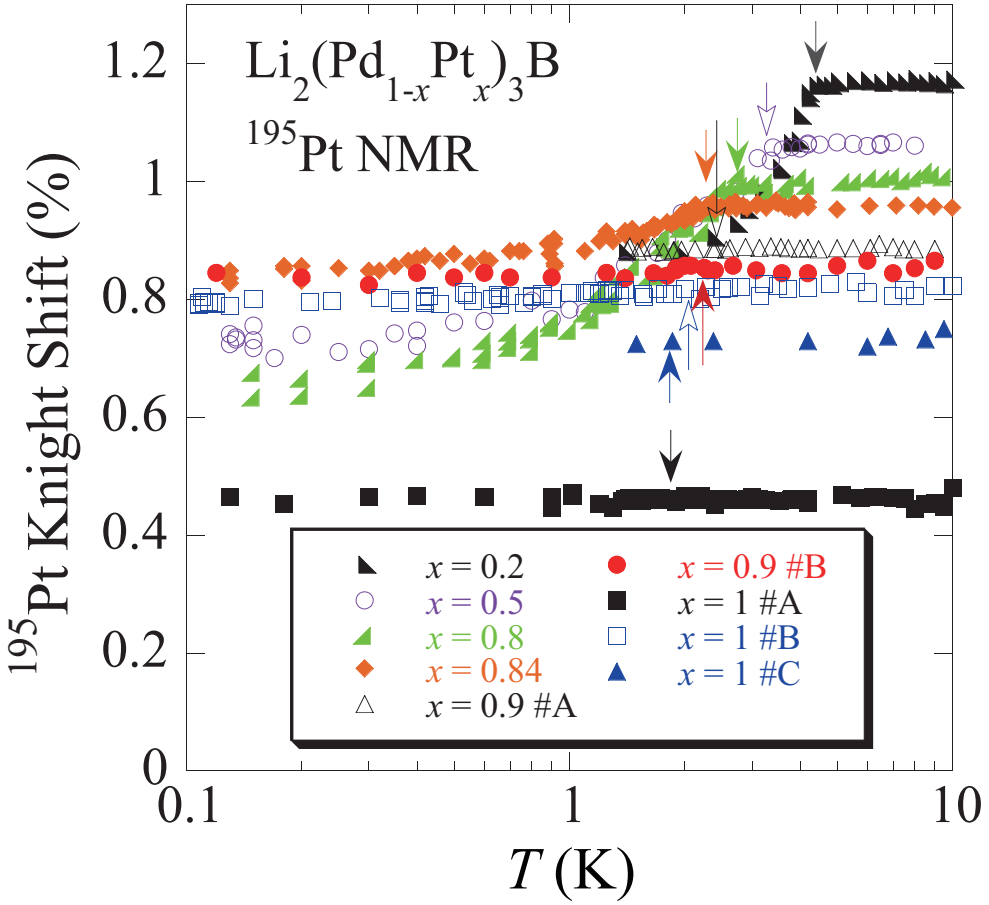

Figure 4.7: Temperature dependence of ^{195}K.

Actually, ^{195}K is composed of spin part and orbital part, $^{195}K = ^{195}K_s + ^{195}K_{orb}$. Therefore, we have to estimate $^{195}K_{orb}$ for accurate discussion of χ_s. However, it can be expected $K_{orb} \sim 0$ using ^{7}Li NMR. It means that ^{195}K is due predominantly to spin susceptibility, χ_s. We could exclude the possiblity that χ_s is nothing for $x \sim 1$.

Figure 4.8 shows K_s^{super}/K_s^{normal} versus x, where K_s^{normal} and K_s^{super} are the Knight shift in a normal state and in the superconducting state (at $T = 0$), respectively. It is found that it is almost constant in $x = 0 - 0.8$ and increases from $x \sim 0.8$. These results imply that the evolution of the triplet component appears from $x \sim 0.8$.

Finally, the K_s^{super} not vanishing completely for $x \leqq 0.8$ can be understood as due to some mixed spin-triplet component and the spin-flip scattering by disorder, and even possible inter-band susceptibility. Indeed, the residual resistivity for the samples of

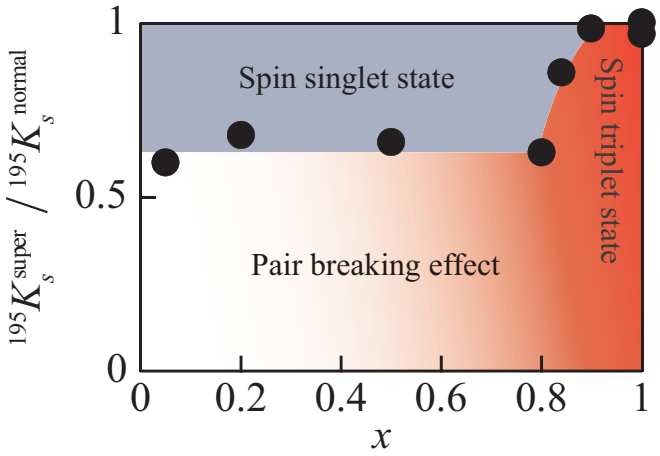

Figure 4.8: $^{195}K(T=0)/^{195}K(T \geq T_c)$ as a fucntion of x.

$0.2 \leqq x \leqq 0.8$ increases substantially compared to the end members, as does the NMR FWHM (Inset of **Fig**. 4.5) which can cause spin-flip scattering for $0.2 \leqq x \leqq 0.8$.

4.2.3 normal state

It is anticipated that some electronic transformations have been occurred by the replacement.

Focusing on the normal state, the compositional dependence of $^{195}(1/T_1T)^{1/2}$ is plotted in **Fig**. 4.9. We found that it decreases smoothly with increasing x but drops sharply for $x \sim 0.8$. Since it is in proportion to DOS at Fermi surface, we can say that the drop comes from that of $N(E_F)$. The possible scenario for the decrease of $N(E_F)$ will be presented in **Discussions**, in which the effect of spin-orbit coupling is discussed.

The decrease of $N(E_F)$ can be seen in ^{195}Pt Knight shift as well, which is given in **Fig**. 4.10. The behavior is consistent with $^{195}1/T_1$ since $^{195}(1/T_1T)^{1/2}$ and ^{195}K have a linear relation ship as a function of x.

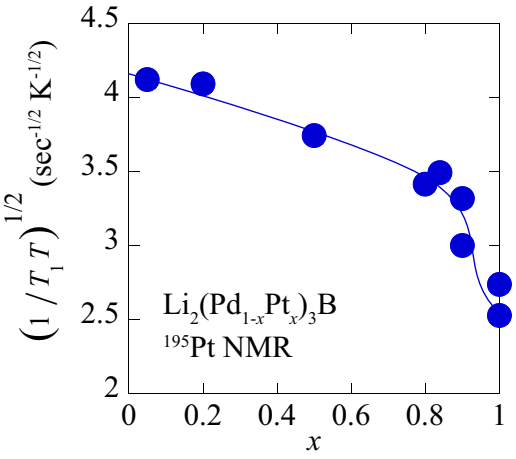

Figure 4.9: $^{195}(1/T_1T)^{1/2}$ as a function of x.

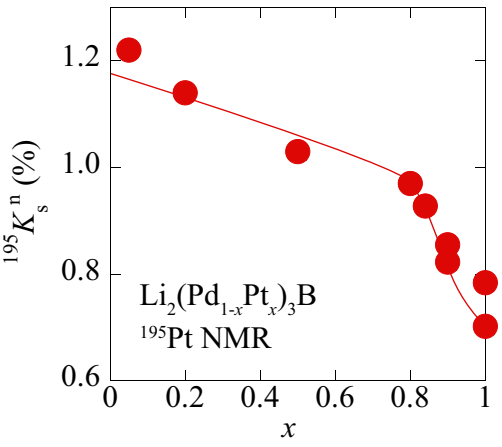

Figure 4.10: ^{195}K as a function of x.

4.3 ^{7}Li NMR

In order to evaluate quantitatively the evolution of χ_s, one needs to know the Knight shift due to orbital susceptibility, $^{195}K_{orb}$, since generally $K = K_{orb} + K_s$, where the spin part K_s is proportional to χ_s or the DOS at the Fermi level, $N(E_F)$.

^{7}Li NMR is useful to estimate the orbital part of ^{195}Pt Knight shift. All ^{7}Li electrons are in s-orbitals meaning that angular momentum is zero ($L = 0$) and share the electronic state with ^{195}Pt electrons. Namely, $^{7}(1/T_1T)^{1/2}$ without orbital contribution mirrors ^{195}K through $N(E_F)$. **Figure** 4.12 gives ^{195}K as a function of $^{7}(1/T_1T)^{1/2}$ in various compositions. It shows a linear relation between ^{195}K and $^{7}(1/T_1T)^{1/2}$. From extrapolation of straight line in **Fig**. 4.12, it is predicted that $^{195}K_{orb}$ is very little and almost all of ^{195}K is composed of $^{195}K_s$.

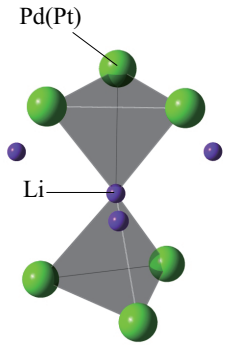

Figure 4.11: Neighborhoods around ^{7}Li

This result strongly supports that the triplet component is dominant for x = 0.9 - 1 because the $^{195}K_s$ remains finite even at very low temperature in the superconducting state. In the spin singlet dominant state for x = 0 - 0.8, the χ_s does not vanish completely. It is thought to be due to the spin-flip scattering [13, 4]. However, in view of this issue, it is more suppressed for x = 0.84 compared to $x \leq 0.8$. This might be because the spin triplet component appears around x = 0.8. The growth of the spin triplet component is very sharp for x, however, it changes continuously, suggesting that the mixing state of the spin singlet and the spin triplet exists above x = 0.8.

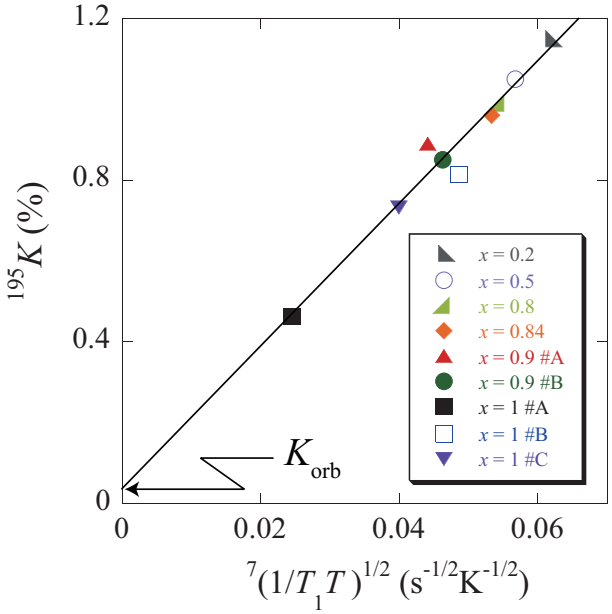

Figure 4.12: ^{195}K versus $^{7}1/T_1T$.

4.4 RietVeld Analysis

4.4.1 lattice constant

RietVeld analysis was performed using the result of XRD [19]. **Figure** 4.13 shows the lattice constant of $Li_2(Pd_{1-x}, Pt_x)_3B$ as a function of x. Sharp contraction of the crystal can be seen from $x \sim 0.8$. The error bars on the plots indicate the fitting error. However, it is noted that the lattice constant for $x = 1$ varies from 6.70 - 6.73Å which depends on the sample quality. Because the synthesis becomes more difficult for $x \geq 0.8$, it may exist a crystal deformations around $x = 1$.

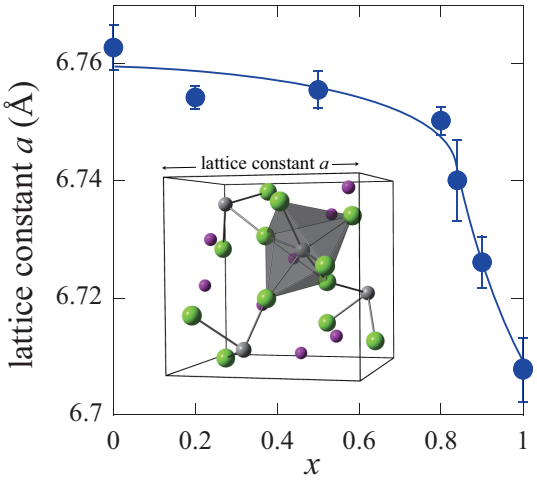

Figure 4.13: lattice constant a as a function of x

4.4.2 octahedral distortion

The octahedral distortion was focused as well. As a gauge to understand the distortion, α and l_{min}/l_{max} were used. The α represents a bond angle between two octahedron at the connection, and l_{min}/l_{max} represents a ratio between the two bond lengths as described in **Fig**. 4.14.

As a result, it is found that the distorted octahedron distorts more for $x \sim 0.8$. Fitting error is within the plots. Instead, approximate error originated from the sample synthesis has been presented.

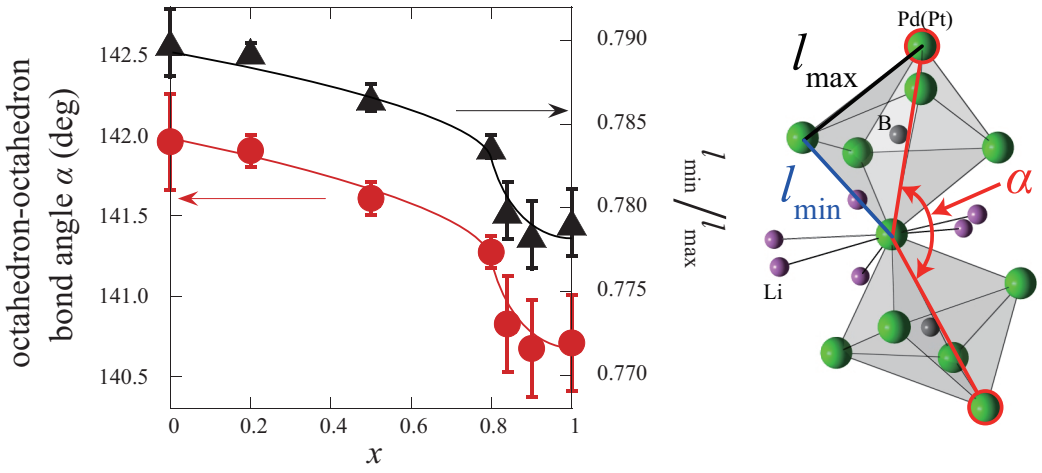

Figure 4.14: Bond angle α and bond length ratio l_{min}/l_{max} as a function of x in distorted octahedral units

From the crystal analysis, it seems that the crystal changes have a strong relation with electronic properties of $Li_2(Pd_{1-x}Pt_x)_3B$.

4.5 Summary of the Results

To summarize the results, what was clarified is indicated again.

(1) Superconducting symmetry in $Li_2(Pd_{1-x}Pt_x)_3B$ changes drastically at $x \sim 0.8$.
For $x \leq 0.8$, the superconducting gap is isotropic and the cooper pair is in spin singlet state. For $x \geq 0.8$, the superconducting gap becomes anisotropic with line node and the cooper pair also becomes spin triplet state.

(2) With increasing x, decrease of density of state was observed
In the normal state, decrease of $^{11}1/T_1$, $^{195}1/T_1$, ^{195}K and $^{7}1/T_1$ were observed. It is expected that their decreases is due to the density of state near Fermi surface. Especially in $^{195}1/T_1$, ^{195}K, the detailed behavior was seen.

(3) Crystal structure changes slightly from $x \sim 0.8$
The lattice constant decrease and crystal distortion is enhanced from $x = 0.8$. It is expected that the changes have a strong relation with above (1), (2).

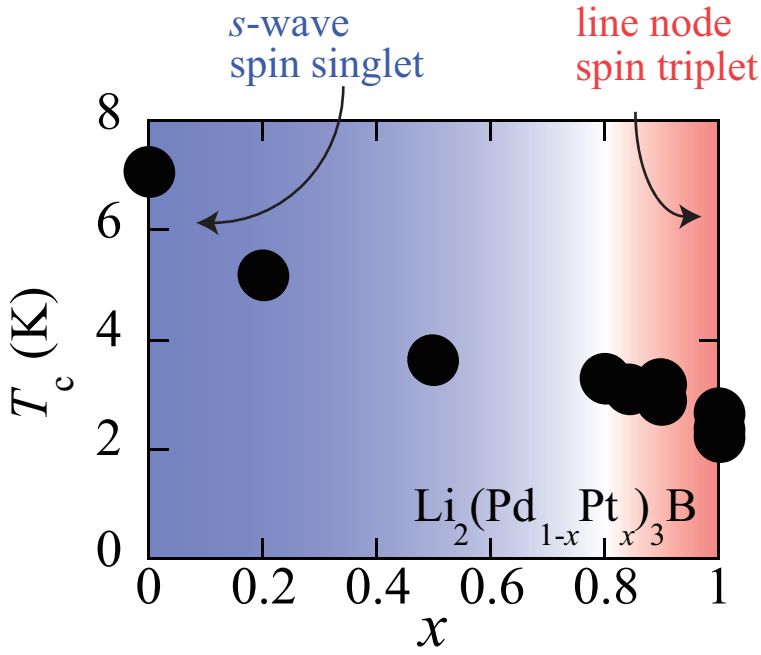

Chapter 5

Discussions

In this chapter, origin of the drastic change of the superconducting properties will be contemplated. The discussion may have some rooms to refine itself, therefore, I hope to get some advice from the standpoint of band calculation. Also, I wish to accelerate the discussion of $Li_2(Pd_{1-x}Pt_x)_3B$ and promote the study of NCS superconductors

5.1 Effect of the Crystal Symmetry on Band Structure of $Li_2(Pd_{1-x}Pt_x)_3B$

The results represents that any physical properties in $Li_2(Pd_{1-x}Pt_x)_3B$ change around $x \sim 0.8$. First at all, I want to explain the origin of the sudden drop of the DOS. Before the explanation, thinking on the band structure will be demanded since the crystal structure is unique.

Once again, we check the crystal structure of $Li_2(Pd_{1-x}Pt_x)_3B$. It has a cubic structure with $P4_332$ in space group. It can be found that there is a spiral axis along with [111] direction. The helical structure are featured in **Fig**. 5.1, which produces a chirality of crystal symmetry. Actually, $Li_2(Pd_{1-x}Pt_x)_3B$ has the right-hand helicity. Therefore, $Li_2(Pd_{1-x}Pt_x)_3B$ is a superconductor with parity breaking symmetry since the right-hand structure can not accord with the left-hand structure.

Using Bloch's theorem, wave function of the right and left hand structures may be given as follows,

$$\Psi^{\text{right}}(\boldsymbol{r}) = \sum_{\boldsymbol{k}} c_{\boldsymbol{k}}^{\text{right}} e^{i\boldsymbol{k}\cdot\boldsymbol{r}} \tag{5.1}$$

$$\Psi^{\text{left}}(\boldsymbol{r}) = \sum_{\boldsymbol{k}} c_{\boldsymbol{k}}^{\text{left}} e^{i\boldsymbol{k}\cdot\boldsymbol{r}} \tag{5.2}$$

where $\boldsymbol{k}$ have all values. We know that the left hand structure is enantiomer of the right hand structures. Therefore, when $\mathcal{P}_r$ is operated into $\Psi^{\text{right}}(\boldsymbol{r})$, it becomes the left-hand helical wave function as follows,

$$\Psi^{\text{left}}(\boldsymbol{r}) = \mathcal{P}_r \Psi^{\text{right}}(\boldsymbol{r}) = \sum_{\boldsymbol{k}} c_{\boldsymbol{k}}^{\text{right}} e^{-i\boldsymbol{k}\cdot\boldsymbol{r}} = \sum_{\boldsymbol{k}'} c_{-\boldsymbol{k}'}^{\text{right}} e^{i\boldsymbol{k}'\cdot\boldsymbol{r}} = \sum_{\boldsymbol{k}} c_{-\boldsymbol{k}}^{\text{right}} e^{i\boldsymbol{k}\cdot\boldsymbol{r}} \tag{5.3}$$

Therefore,

$$\Psi^{\text{left}}(\boldsymbol{r}) \equiv \sum_{\boldsymbol{k}} c^{\text{left}}_{\boldsymbol{k}} e^{i\boldsymbol{k}\cdot\boldsymbol{r}} = \sum_{\boldsymbol{k}} c^{\text{right}}_{-\boldsymbol{k}} e^{i\boldsymbol{k}\cdot\boldsymbol{r}} \tag{5.4}$$

$$\Longrightarrow c^{\text{left}}_{\boldsymbol{k}} = c^{\text{right}}_{-\boldsymbol{k}}. \tag{5.5}$$

We could get the relation of the coefficients (**Equation** 5.5).

In our world, only the right hand structure exsits whereas the left hand structure does not, which can exist only in the mirror. Namely, the $\Psi^{\text{right}}(\boldsymbol{r})$ is a real wave function and the $\Psi^{\text{left}}(\boldsymbol{r})$ is a virtual wave function. From any viewpoints, right hand structure has the right hand chirality not the left hand chirality. Since we do not need to be nervous about the virtual mirror world, we can assume

$$\Psi^{\text{left}}(\boldsymbol{r}) = \mathcal{P}_r \Psi^{\text{right}}(\boldsymbol{r}) \equiv 0. \tag{5.6}$$

Using the **Equation** 5.5, it produces

$$c^{\text{left}}_{\boldsymbol{k}} = c^{\text{right}}_{-\boldsymbol{k}} = 0 \tag{5.7}$$

, implying that

$$E^{\text{right}}_{-k} \equiv \sum_{k'} \langle k'|\mathcal{H}|-k\rangle \tag{5.8}$$

$$= 0 \tag{5.9}$$

where k is a wave number which characterizes the chirality. The band structure may be described using only $k \geqq 0$ space (or $k \leqq 0$ space). Therefore, **Fig**. 1.4 (b) will be refined into **Fig**. 5.2 (c) as a expected band structure. We can gess that there is a single band with broken spin degeneracy in the Fermi surface. Incidentally, $CePt_3Si$ have both Ψ and $\mathcal{P}_r\Psi$ in reality, therefore, there is a double split bands which have an opposite direction of spin each other. It may give physical differences between $Li_2(Pd_{1-x}Pt_x)_3B$ and $CePt_3Si$.

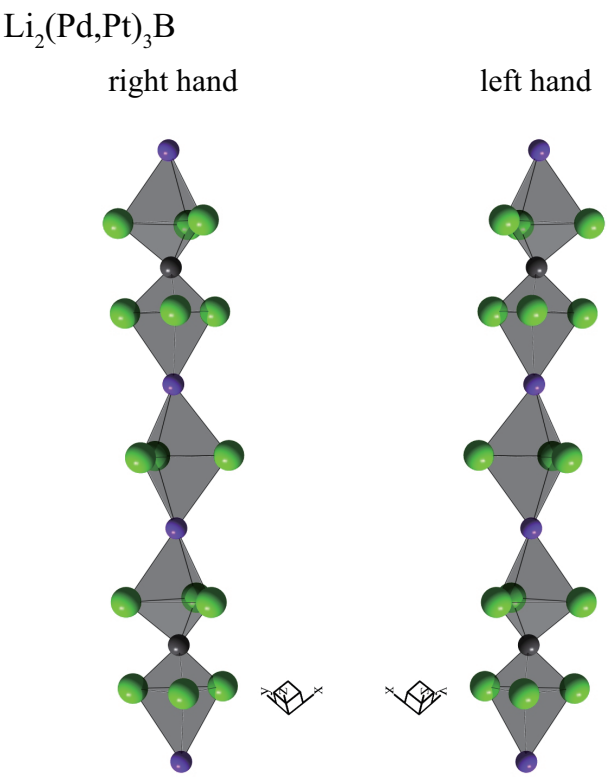

Figure 5.1: Right and left hands helical structure in $Li_2(Pd,Pt)_3B$. Actually, $Li_2(Pd,Pt)_3B$ has a right hand helical chirality.

Figure 5.2 represents the outline of the band structure of two situations with weak and strong spin-orbit coupling. In **Fig**. 5.2 (a), strong spin-orbit interaction will make either up spin or down spin survive at the Fermi surface. In contrast in **Fig**. 5.2 (c) with weak spin-orbit interaction, the broken bands will get closer each other and thus both up and down spins may exist within a given energy scale.

The followings may be unnecessary to add but the circumstance that either up or down spin runs over the Fermi surface, may be an important factor of novel spin triplet pairing for Li_2Pt_3B.

Figure 5.2 (b), (d) shows their DOS for **Figure** 5.2 (a), (c), respectively. If their Fermi energy is at the dotted line in **Fig**. 5.2, decrease of DOS is expected by the

enhancement of the spin-orbit interaction which produces the splitting of the spin-degenerate band near E_F. In my NNR results, the decreases of DOS was observed for $x \geqq 0.8$, which gives experimental support to the above hypothesis and suggests that the spin-orbit interaction is suddenly dynamized.

5.2 Consideration of the Rietveld Analysis

In this section, I discuss the relations between the superconducting symmetry and the crystal structure analysis. I want to consider two situations, for $x > 0.8$ and $x \leqq 0.8$ since their superconducting properties are completely different.

5.2.1 $x > 0.8$

It can be understood that the drop of DOS is due to the enhancement of the spin-oribt coupling. Then, what is the origin of the enhancement? We can expect that it is (1) atomic number, Z or (2) symmetry breaking. From **Fig**. 4.14, the sharp enhancement of crystal distortion around $x = 1$ was confirmed. It will promotes the drastic development of the spin-orbit interaction, $\alpha g_k \bullet \sigma \equiv \sum_{k'} \langle k' | \lambda \boldsymbol{L} \bullet \boldsymbol{S} | k \rangle$ since high symmetry kills the $\alpha g_k \bullet \sigma$ while the distortion produces the finite interaction (**section 1.8**). This results let us take the origin as (2) symmetry breaking. The smooth displacement of Pd for Pt namely smooth increase of Z cannot simply explain the sharp enhancement of the spin-orbit interaction.

Namely, by the enhancement of the distortion, Li_2Pt_3B will get the strong spin-orbit interaction which largely separate the spin degeneracy like **Figure** 5.2 (a). From my NMR results, the conventional superconductivity for $x = 0$ - 0.8 have been transformed to the novel line node, spin triplet state with enhancing the distortion (with increasing x). Therefore, we can get a clear interpretation for $x = 0.8$ - 1 that the mixed superconducting symmetry were controlled by the $\alpha g_k \bullet \sigma$. As a result, it can be concluded that the mixing of spin singlet and triplet states appears in $0.8 < x < 1$, which are controlled by the crystal distortion.

Actually, more detailed insight will be required for the mixing of the spin singlet and triplet states. At least, it can be said that the unique crystal inversion symmetry breaking, rather than the large atomic number, has no small effect on the novel spin symmetry. Namely, broken inversion symmetry is an indispensable element.

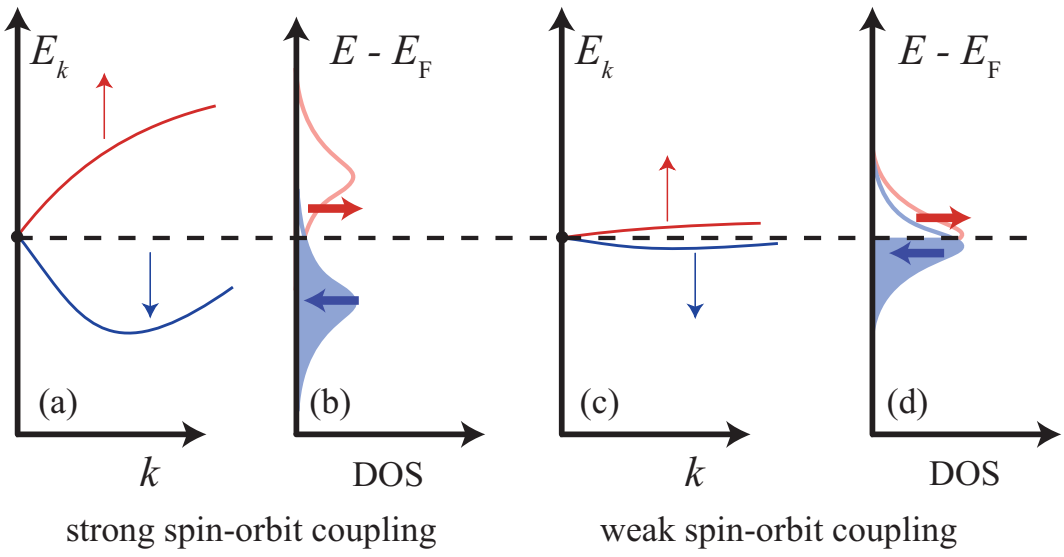

Figure 5.2: Sketch of the expected band structure in $Li_2(Pd_{1-x}Pt_x)_3B$.

5.2.2 $x \leqq 0.8$

Actually, increase of α (or λ) by replacement of Pd for Pt also gives the development of the $\alpha g_k \bullet \sigma$. Therefore, the $\alpha g_k \bullet \sigma$ will change with increasing x (= 0 - 0.8), even if the distortion remains unchanged. However, the superconducting symmetry for $x = 0 - 0.8$ shows no clear changes from the NMR results. It is interesting from viewpoint of the previous discussion because that means the superconducting symmetry is independent of the spin-orbit interaction. To explain this, it is reasonable to consider that the superconducting background is completely different from $x = 0.8$ as a border.

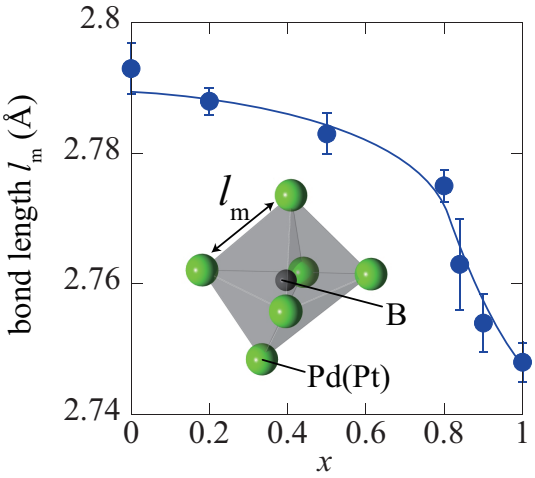

Figure 5.3: Lattice constant a as a function of x

The above discussion has been conducted under a assumption that Fermi energy is in the separated band structure. If the Fermi energy is in the other band, we can not take the constant discussion.

Ordinarily, the Fermi energy depends on the coulomb potential $V(r)$. It produces the orbital character like s, p, d, f,... However in a heavy atom, the theory of relativity have to be taken into account as it is discussed in **section 1.5**. Therefore, the actual Fermi energy is determined by both $V(r)$ and the spin-orbit interaction, $\Lambda [\nabla V(r) \times \boldsymbol{p}] \bullet \sigma$. (This relativity effect makes it difficult to describe band structure in heavy element.)

Therefore, the given Hamiltonian is

$$\mathcal{H} = \frac{p^2}{2m} + V(r) + \Lambda [\nabla V(r) \times \boldsymbol{p}] \bullet \sigma. \tag{5.10}$$

As the eigen wave function Φ, the **Equation** (1.72) are used, Therefore,

$$\begin{aligned} E &= \langle \Phi | \mathcal{H} | \Phi \rangle && (5.11) \\ &= \langle J, M | \mathcal{H} | J, M \rangle \\ &\quad + \sum_{kk\sigma} \sum_{k',\sigma'} c^*_{k',\sigma'} c_{k,\sigma} \langle k', \sigma' | \mathcal{H} | k, \sigma \rangle && (5.12) \\ E &= E_F + \sum_{k,\sigma} \sum_{k',\sigma'} c^*_{k',\sigma'} c_{k,\sigma} \langle k', \sigma' | \mathcal{H} | k, \sigma \rangle && (5.13) \end{aligned}$$

where

$$\begin{aligned} E_F &= \langle J, M | \mathcal{H} | J, M \rangle && (5.14) \\ &= \left\langle J, M \left| \frac{p^2}{2m} + V(r) \right| J, M \right\rangle + \langle J, M | \lambda \boldsymbol{L} \bullet \boldsymbol{S} | J, M \rangle && (5.15) \\ &= E_0 + \lambda \{ J(J+1) - L(L+1) - S(S+1) \} && (5.16) \end{aligned}$$

The **Equation** (5.13) represents that the free electrons move on the E_F as the **Equation** (5.16). Whichever electronic state is in the less than half-full or more than half-full, the spin-orbit coupling $\lambda \{ J(J+1) - L(L+1) - S(S+1) \}$ gives a negative value. Therefore, the E_F gives a high energy state with decreasing λ. This is wrong situation

for electrons. The electrons will seek the other energy band which can ease the situation such as s-band. This is since s-band is unaffected by the spin-orbit interaction; besides it is a extended band with respect to energy and thus it exists anywhere. As a result, it is anticipated that the spin degenerate s-band in the Fermi surface contributes to the unchanged superconducting symmetry for $x = 0$ - 0.8.

To enforce the discussion, the change of the lattice constant in **Figure** 4.13 will be used. The lattice constant gives an information of actual bond length. **Fig** 5.3 shows the bond length l_m between the nearest Pd(Pt). It can be seen that the l_m increases with decreasing x. Namely, distance between Pd(Pt)-Pd(Pt) expands. It is expected that mean radius of Pt in $6s$-orbital is larger than that of $5d$-orbital. Therefore, the change of the Pt electric orbital causes that of metallic distance from standpoint of the previous discussions.

Incidentally, the radii of simple metals, Pd and Pt are 1.37 and 1.39Å, [27]. The reason why the two different metallic radii are similar, is due to that nuclear core potential of Pt is stronger than that of Pd which causes orbital shrink for Pt.

5.3 Summary of the Discussion

As summary of the above discussions, it is convenient to think the phenomena for $x > 0.8$ and $x \leqq 0.8$, separately. For, $x > 0.8$, the crystal distortion controls the superconducting symmetry and decrease of density of state near Fermi surface. For, $x \leqq 0.8$, the change of the electronic orbital to s-state makes the superconducting symmetry unchanged. Both phenomena are due to the spin-orbit interaction which changes the electronic environment (**Fig**. 5.4). These expectation were enforced by crystal analysis.

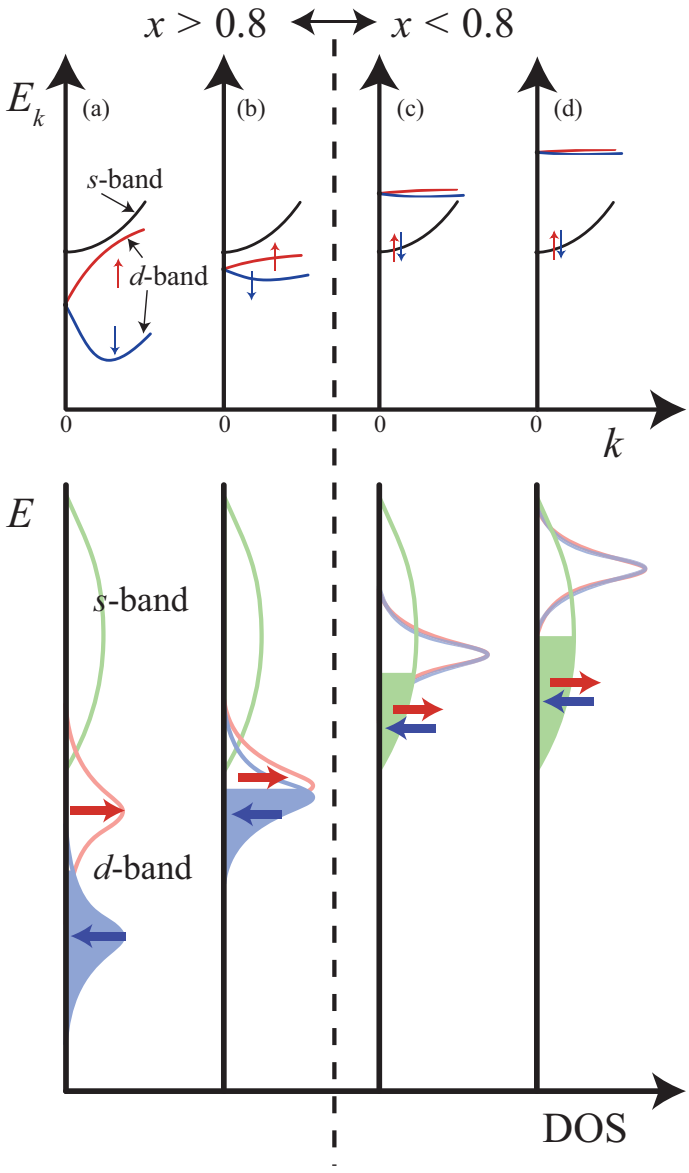

Figure 5.4: Sketch of the band structure for $x > 0.8$ and $x \leqq 0.8$. The difference is that electrons move on d-orbital in which the spin degeneracy has been broken for $x \geq 0.8$ or move on s-orbital for $x \leqq 0.8$.

Chapter 6

Conclusion

In conclusion, I studies the evolution of Cooper pair's symmetry by tuning the spin-orbit interaction in $Li_2(Pd_{1-x}Pt_x)_3B$.

I synthesized the sample of $Li_2(Pd_{1-x}Pt_x)_3B$ ($x = 0, 0.2, 0.5, 0.8, 0.84, 0.9, 1$) which were checked by XRD and also, the superconductivity. The quality of the samples coincides with that of the previous report. It was found that all the samples were successfully prepared.

By means of NMR, it is found that the pairing symmetry changes drastically at $x = 0.8$. The $^{11}(1/T_1)$ has a coherence peak for $x \leq 0.8$ but no coherence peak for $x \geq 0.9$ being consistent with $^{195}(1/T_1)$. In addition, it is found residual density of state for $^{195}(1/T_1)$ at low temperature which insists nodal gap behavior. Also, ^{195}K for $x \leq 0.8$ decreases below T_c whereas does not decrease for $x \geq 0.9$. For $x \leq 0.8$, the materials are in a predominantly spin-singlet state. However for $x > 0.9$, unconventional properties due to the development of the spin triplet state appear. For $x = 0.84$, the mixing-like behavior was observed. Furthermore, I found the sudden decrease of the density of state at Fermi surface and suggest that it is due to enhancement of the spin-orbit interaction which breaks the spin degeneracy.

From the crystal analysis, the sudden enhancement of the spin-orbit interaction has been produced by an increased distortion of the $BPd(Pt)_6$ octahedral units which were characterized by α and $l_{\min}/l_{\max}$. My results indicate that, in addition to a large Z, the structure distortion as to increase the extent of inversion-symmetry breaking is another important, and more effective factor to increase the mixing of the spin-triplet state.

In addition to that, the drastic change of the superconducting symmetry depends on environment near Fermi surface which is also controlled by the spin-orbit interaction. These effects are not targeted in only superconductor but topological insulator, spintronics devise, maltiferroics and so on. It provide a good opportunity for future studies on this new direction of condensed matter physics.

Bibliography

[1] T. Akazawa, H. Hidaka, T. Fujiwara, T. C. Kobayashi, E. Yamamoto, Y. Haga, R. Settai, and Y. Ōnuki, J. Phys. Cond. Matt. **16** (2004) L29.

[2] G. Adachi, (1999) "*Kidorui no kagaku*" kagakudojin.

[3] K. Asayama, (2002)
"*Henrekidensikei no kakujikikyomei -kinzokujisei to chodendo-*" Shokabo.

[4] P. W. Anderson, Phys. Rev. Lett. **3** (1959) 325.

[5] P. W. Anderson, Phys. Rev. **115** (1959) 2.

[6] P. Badica T. Kondo, and K. Togano, J. Phys. Soc. Jpn. **74** (2005) 1014.

[7] E. Bauer, G. Hilscher, H. Michor, Ch. Paul, E. W. Scheidt, A. Gribanov, Yu. Seropegin, H. Noël, M. Sigrist and P. Rogl, Phys. Rev. Lett. **92** (2004) 027003.

[8] E. Bauer, R. T. Khan, H. Michor, E. Royanian, A. Grytsiv, N. Melnychenko-Koblyuk, P. Rogl, D. Reith, R. Podloucky, E.-W. Scheidt, E.-W. Scheidt and M. Marsman, Phys. Rev. B **80** (2009) 064504.

[9] Charles E. Burkhardt and Jacob J. Leventhal (2008)
"*Foundations of quantum physics*" Springer.

[10] M. K. Crawford, M. A. Subramanian, R. L. Harlow, J. A. Fernandez Baca, Z. R. Wang and D.C. Johnston, Phys. Rev. B. **49** (1994) 9198.

[11] U. Eibenstein and W. Jung, J. Solid State Chem. **133** (1997) 21.

[12] G. Eguchi, D. C. Peets, M. Kriener, Y. Maeno, E. Nishibori, Y. Kumazawa, K. Banno, S. Maki and H. Sawa, Phys. Rev. B. **83** (2011) 024512.

[13] R. A. Ferrel, Phys. Rev. Lett. **3** (1959) 262.

[14] P. A. Frigeri and D. F. Agterberg and A. Koga M. Sigrist,
Phys. Rev. Lett. **92** (2004) 097001.

[15] S. Fujimoto, J. Phys. Soc. Jpn. **76** (2007) 034712.

[16] L. P. Gorkov, and E. I. Rashba, Phys. Rev. Lett. **87** (2001) 037004.

[17] S. Koide. (2004) "*Ryoshirikigaku* (II)" Shokabo.

[18] M. Itoh, T. Shimura, Y. Inaguma and Y. Morii J. Solid State Chem. **118** (1995) 206.

[19] F. Izumi and T. Ikeda, Mater. Sci. Forum, **321-324** (2000) 198.

[20] B. J. Kim, H. Ohsumi, T. Komesu, S. Sakai, T. Morita, H. Takagi, T. Arima,
Science **323** (2009) 1329.

[21] N. Kimura, K, Ito, K. Saitoh, Y. Umeda, H. Aoki, and T. Terashima, Phys. Rev. Lett. **95** (2005) 247004.

[22] T. Klimczuk, Q. Xu, E. Morosan, J. D. Thompson, and J. D. Thompson, Phys. Rev. Lett. **74** (2006) 220502(R).

[23] T. Konno, (2001) "*Bussitu no taishosei to gunron*" Kyoritsushuppan

[24] J. Matsuno, Y. Okimoto, Z. Fang, X. Z. Yu, Y. Matsui, N. Nagaosa, M. Kawasaki, and Y. Tokura, Phys. Rev. Lett. **93** (2004) 167202.

[25] T. Moriya, Phys. Rev. Lett. **4** (1960) 228.

[26] T. Moriya, Phys. Rev. **120** (1960) 91.

[27] National Astronomical Observatory of Japan. (ed) (2005) "*Chronological science tables*" Maruzen.

[28] M. Nishiyama, Y. Inada, and Guo-qing Zheng, Phys. Rev. B **71** (2005) 220505(R).

[29] M. Nishiyama, Y. Inada, and Guo-qing Zheng, Phys. Rev. Lett **98** (2007) 047002.

[30] K. V. Samokhin, Phys. Rev. Lett., **94** (2005) 027004.

[31] T. Shibayama, M. Nohara, H. Aruga Katori, Y. Okamoto, Z. Hiroi, H. Takagi, J. Phys. Soc. Jpn. **76** (2007) 0730708.

[32] Sk. Md. Shamsuzzaman, Y. Inada, S. Sasano, S. Harada, G.-Q. Zheng, Journal of Physics: Conference Series **200** (2010) 012183.

[33] C. P. Slichter, (1996) "*Principles of magnetic resonance*" Springer

[34] I. Sugitani, Y. Okuda, H. Shishido, T. Yamada, A. Thamizhavel, E. Yamamoto, T. D. Matsuda, Y. Haga, T. Takeuchi, R. Settai, and Y. Ōnuki, J. Phys. Soc. Jpn. **75** (2006) 043703.

[35] H. Takeya, M. ElMassalami,S. Kasahara, and K. Hirata, Phys. Rev. B **76** (2007) 104506.

[36] H. Takeya, K. Hirata, K. Yamaura, and K. Togano, M. El Massalami, R. Rapp, and F. A. Chaves, B. Ouladdiaf, Phys. Rev. B **72** (2005) 104506.

[37] K. Tahara, Z. Li, H. X. Yang, J. L. Luo, S. Kawasaki, and Guo-qing Zheng, Phys. Rev. B **80** (2009) 060503(R).

[38] K. Togano, P.Badica, Y. Nakamori, S. Orimo, H. Takeya, and K.Hirata, Phys. Rev. Lett **93** (2004) 247004.

[39] J. Yan, L. Shan, Q. Luo, W.-H. Wang, and H.-H. Wen, Chinese Phys. B **18** (2009) 704.

[40] T. Yokoya, T. Muro, I. Hase, H. Takeya, K. Hirata, and K. Togano, Phys. Rev. B **71** (2005) 092507.

[41] M. Yogi, Y. Kitaoka, S. Hashimoto, T. Yasuda, R. Settai, T. D. Matsuda, Y. Haga, Y. Ōnuki, P. Rogl and E. Bauer, Phys. Rev. Lett. **93** (2004) 027003.

[42] M. Yogi, H. Mukuda, Y. Kitaoka, S. Hasimoto, T. Yasuda, and R. Settai, T. D. Matsuda, Y. Haga, Y. Ōnuki, P. Rogl and E. Bauer, J. Phys. Soc. Jpn. **75** (2006) 013709.

[43] R. Yoshida, H. Okazaki, K. Iwai, Noami, T. Muro, M. Okawa, K. Ishizaka, S. Shin, Z. Li, J. L. Luo, G. Q. Zheng, T. Oguchi, M. Hirai, Y. Muraoka, and T. Yokoya, J. Phys. Soc. Jpn. **78** (2009) 034705.

[44] H. Q. Yuan, D. F. Agterberg, N. Hayashi, P. Badica, D. Vandervelde, K. Togano, M. Sigrist, and M. B. Salaamon, Phys. Rev. Lett. **97** (2006) 017006.

Acknowledgment

I would like to express special thanks to Professor G.-q. Zheng for giving the fruitful assignment and suggestions about the research and technical problems of NMR and providing enough funding and chance to study, Professor Y. Inada for teaching the way of the synthesis and chemical composition analysis such as EDX and atomic absorption and also for giving considerable suggestions, Professor K. Asayama for providing useful comments on the NMR results as an expert in this field, Lecturer S. Kawasaki for helps in some measurements and NMR analyses, Dr. K. Matano for helps in technical problems, Dr. F. Iwase for giving an insight and bringing a breath of fresh air into our laboratory, Dr. Z. Li for coaching XRD analysis and building up my English communication skills as well as Mr. Sk. Md. Shamsuzzaman who taught the procedure of the synthesis and resistivity and magnetization measurements. I also thank he or she who has not been mentioned here.

Finally, I am very thankful to my father and mother for financial and mental supports over the 9-years. With no exception, I appreciate everyone who had been involved with my academic life.